Simulation-based Design of In-Plane Switching Liquid Crystalline Display Pixels

by

Anindya Mitra

A thesis
presented to the University of Waterloo
in fulfillment of the
thesis requirement for the degree of
Master of Applied Science
in
Chemical Engineering

Waterloo, Ontario, Canada, 2016

I hereby declare that I am the sole author of this thesis. This is a true copy of the thesis, including any required final revisions, as accepted by my examiners.

I understand that my thesis may be made electronically available to the public.

Abstract

Liquid crystal displays (LCDs) constitute an important class of modern display technologies. Their light-weight nature, coupled with their favourable power consumption characteristics make them useful in applications ranging from large area projection displays to small electronic devices such as digital watches and calculators.

Despite being the market leader in the display industry, traditional configurations of LCDs suffer from serious drawbacks such as having a very narrow viewing cone. Newer configurations of LCDs, however, employ the in-plane switching (IPS) mode and its derivatives. These provide a much wider viewing cone with lower degradation of image quality as one moves off the central axis.

IPS pixels have a unique configuration as they contain the electrodes on only one side of the domain. The electrodes are arranged in an interdigitated pattern and produce an electric field that varies periodically in space parallel to the substrates and decays exponentially in space along the through-plane direction.

The highly non-homogeneous nature of the electric field makes the simulation of the electric field within an IPS domain more challenging as a minimum of two dimensions is needed to model the electric field with sufficient accuracy, in contrast to the electric field in the twisted nematic (TN) mode that may be modelled in only one dimension. Traditional approaches have employed an iterative technique wherein the Gauss law equations are solved for a pre-determined director configuration and the electric field thus obtained is employed to calculate the new director configuration over the domain. The iterations are continued till convergence is attained.

Our method involves calculating the electric field by means of a semi-analytical expression for an electric field produced by interdigitated electrodes and using this expression to calculate the domain configuration. This methodology is advantageous in terms of computational time and effort as it gives a possible way to do away with the back and forth iterations involving the dynamic equations and the Gauss' law equations. In this work, we attempt to look at dynamic characteristics of the liquid crystalline domain in an IPS-LCD. Metrics were evolved to quantify the deformation in the domain. Finally, these metrics were used to examine the dependence of the equilibrium orientation on the domain thickness, electrode width, electrode spacing and electric voltage applied.

The results show good match with the trends that can be expected from theoretical considerations. The variation of the domain deformation characteristics with the change in the geometric and physical parameters is along expected lines. For instance, increasing

the voltage results in the domain getting deformed to a much greater extent and the deformation to penetrate deep within the domain. A greater pixel depth with the same values of the other parameters results in more of the domain staying undeformed as the electric field only penetrates upto a fixed distance into the domain. Increase in the electrode spacing was not found to make a significant contribution to the deformation while increasing the width of the electrodes increases the area affected by the electric field and thus, this increases the overall deformation.

To conclude, the framework provided here is a valid first step in evolving a complete software package to model deformation characteristics of an LCD pixel. The code is flexible enough to accommodate different LCD configurations and thus, may be used to model a variety of other LCD configurations also. A parallel development of an optics code using a matrix based method may be used to model the propagation of light through the domain and this may be added very easily on top of the existing framework to create a complete package for analysing the electro-optical properties of the LCD.

Acknowledgements

I would like to sincerely thank my supervisor, Prof. Nasser Mohieddin Abukhdeir for his unwavering support, guidance and motivation throughout the course of the project.

I would also like to thank other members of the Abukhdeir Research Group (ARG), particularly Tanyakarn Treeratanaphitak, Fred Fu, Ryan Neufeld, Grigoriy Kimaev, Donya Ahmadi and Kai Kim with whom I have had the pleasure of working with over the course of my Masters.

I would also like to acknowledge the support and encouragement received from my friends Raktika, Manikuntala, Tanusree, Rajdip, Subhajit and many others without which this work would not have been possible.

Dedication

Dedicated to my grandmother, Anjali Deb.

Table of Contents

List of Figures

Nomenclature

α	Surface anchoring energy density
η_{tilt}	Tilt metric
η_{twist}	Twist metric
$\mathbf{I}$	Identity Tensor
$\mathbf{n}$	Director
$\mathbf{Q}$	Alignment tensor
τ	Dimensionless time
$\varepsilon_{\perp}$	Dielectric constant perpendicular to the director
a	$s+w$
A, B, C	Coefficients of thermodynamic terms in the Landau-de Gennes expansion
d	Pixel depth
f	Free energy density
J_0	Bessel's function
K_{11}	Frank's *splay* elastic constant
K_{22}	Frank's *bend* elastic constant
K_{33}	Frank's *twist* elastic constant
L_1, L_2, L_3	Coefficients of elastic energy terms in the Landau-de Gennes expansion

n_e	Refractive index for the extraordinary ray
n_o	Refractive index for ordinary ray
S	Scalar Order Parameter
s	Electrode spacing
T_{NI}	Temperature at which the nematic phase becomes more stable than the isotropic phase
V_0	Applied voltage
w	Electrode width

Chapter 1

Introduction

1.1 Motivation

The global display industry is worth approximately one hundred billion dollars at present. Although cathode ray tube (CRT)-based displays were the dominant market leader in this industry at the close of the 20^{th} century , liquid crystal displays (LCDs) have gradually taken over the position as leader, occupying about 90% of the total market. [1]. LCDs are ubiquitous in a variety of display applications such as television screens, desktop and laptop computers, mobile phone displays and large area displays.

The main advantage of LCDs that allowed them to overtake CRTs in the display industry is their compact size and lighter weight. In fact, the overall size of CRT-based television screens and computer display monitors were limited mostly on account of the bulkiness of the associated vacuum tube. CRT display screens also require a very thick shielding (mostly made of leaded glass to protect the user from x-rays) that added further bulk and weight to the CRT display. LCD pixels achieve a comparable resolution, on the other hand, but only are a few microns thick, greatly reducing the overall thickness of the entire display panel. Furthermore, unlike CRTs, [18] no exposure to x-rays occurs with an LCD panel. Environmental concerns related to the disposal of the CRT monitors on account of the presence of lead [19] also do not exist with LCD panels.

A major drawback of early LCD technology was a narrow viewing angle with the viewing quality declining sharply as one moved off the central axis. This was due to a drawback in the twisted nematic (TN) mode used in early LCD displays that allowed light to pass through the LC domain without encountering a change in its state of polarisation, especially at high viewing angles.

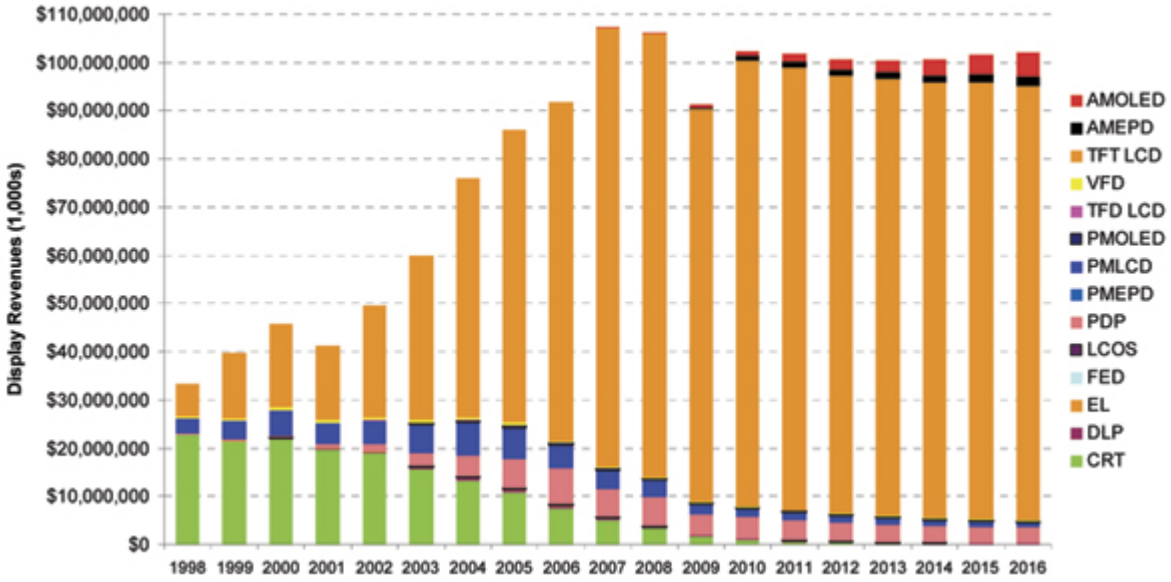

Figure 1.1: A graphic showing the relative market shares of different types of display technologies. TFT-LCD (thin film transistor-liquid crystal display) largely displaced CRTs to become the market leader by the middle of the first decade of the 21^{st} century. CRTs were virtually rendered obsolete by the end of the first decade [1].

In other words, in order for the light to be transmitted through the display pixel, it is essential for the light to encounter birefringence in the LC domain. Birefringence refers to the phenomena wherein an optical media has two different refractive indices. Most LC materials used in LCDs are *calamitic*, or rod-shaped in nature. In order for such molecules to show birefringence, the light needs to strike them side on. Light striking such molecules parallel to its optical axis (end on), encounters only one index of refraction and thus, no birefringence. This causes the exit polariser to block off this light and thus, the LCD pixel employing the TN configuration has a very narrow viewing cone.

Evolution of technologies such as in-plane switching (IPS), fringe field switching (FFS) and multiple vertical alignment (MVA) have improved the viewing angle characteristics of LCD displays significantly to the point where they are being used even in large area projection displays.

It is important to understand that LCD pixels are *passive* displays in contrast to technologies such OLEDs (organic light emitting diode). LCD pixels merely modify the light

that passes through them and do not produce their own light. Back light panels, increasingly made of LEDs these days, are used to illuminate the LCD pixel. This introduces an inherently finite contrast ratio, defined as the ratio of intensity of a fully dark pixel to a fully bright pixel. In contrast, the contrast ratio of an active display such as OLED (that produces its own light) is theoretically infinite, as in the dark state, the light source can be simply turned off, making the intensity in the dark state zero. However, OLEDs are still far from reaching the technological maturity of LCDs and at present are manufactured by only a small number of companies. Furthermore, OLEDs are generally far more expensive at present than LCDs.

Essentially, an LCD pixel can be thought of being a light-valve that is actuated electrically. The main functional elements of an LCD pixel include a set of back-lights, a set of crossed polarisers placed at two ends of the pixel and transparent electrodes to actuate the LC domain. The LC material is sandwiched in between. By a phenomenon known as *wave-guiding*, the polarisation vector of light changes orientation as it passes through the domain. Final intensity depends on angle between the polarisation vector of light and the optic axis of the second polariser ($I = I_0 \cos^2 \theta$).

The exact anatomy of an LCD pixel depends upon its type. For instance, IPS pixels contain only one set of electrodes while TN (twisted nematic) pixels use electrodes on both sides of the pixel domain. Different geometric and physical parameters, such as the depth of the LCD pixel and the strength of the electric field used for actuation of the domain affect the overall transmittance of an LCD pixel. These parameters often interact in complex ways and thus an optimal design needs to be fabricated in order for the pixel to give the best output.

Over time, a number of different configurations of the LCD pixel have been proposed [20]. The twisted nematic (TN), was, for a very long time, the most widely used mode. The TN pixel domain consists of a uniform LC domain twisted uniformly over the pixel domain by an angle of $\frac{\pi}{2}$ radians and electrodes on two ends of the domain. Wave-guiding by the LC domain in the OFF state causes the polarisation vector to twist across the domain and thus pass through the second polariser without any obstruction. In the ON state, the electric field produced by the electrodes on the two ends cause the LC molecules to align vertically. This breaks the wave-guiding property of the domain and thus the light gets blocked by the second polariser.

The TN mode had a very narrow viewing angle so that the off-axis image quality was poor as compared to other technologies. This means that the image characteristics appeared fine if one looked at a pixel directly from the front, but the image quality degraded sharply if one moved from side to side or up/down. This was due to the fact that for larger

viewing angles, the LC domain appeared optically isotropic. Modifications to the pixel design led to the evolution of newer configurations such as IPS that had better viewing angle characteristics and were also lighter owing to the fact that the electrodes were present on only one side of the domain.

The electric field produced by the electrodes in a configuration such as the TN is much simpler as it is uniform throughout the domain. Thus, TN pixels may be modelled in a single dimension with sufficient accuracy. On the other hand, in the IPS mode, the electric field is considerably more complicated and varies spatially in both the in-plane and the through-plane directions [21]. Thus, at least a two dimensional simulation must be carried out to accurately model the pixel behaviour with sufficient accuracy.

Simulation-assisted studies of an engineering system allow different combinations of these parameters to be tested at much lower cost than in an experimental setting and allow one to gain valuable feedback regarding the interactions between these factors and their overall effect on the system before the system is even constructed. Furthermore, these studies help to consider the engineering problem from a number of different levels of detail. A crude design of the system may be carried out by modelling individual components only as black boxes. Once this is accomplished, additional levels of detail and complexity may be introduced [22]. Simulation-based studies also allow us to undertake much more detailed studies of the exact texture and deformation of the LC domain. For instance, rather than inferring the domain orientation from the output transmittance, our simulations allow us to exactly model and investigate the spatial orientation of the domain. Further details are provided in later chapters. Whilst a number of commercial software packages have been developed that can provide detailed simulations of these domains, they are in general expensive and not accessible in an academic environment. This is one of the reasons that a new open source code had to be evolved during the course of this project.

The simulation of the operation of an LCD pixel in general involves two major steps. The first step involves simulating the deformation of the LC domain due to the application of an electric field. The second step then involves the use of this equilibrium configuration of the LC domain and simulating the propagation of light through the domain. Two common approaches can be used, the first involves finding solutions to Maxwell's equations numerically. The FDTD (finite difference time domain) and the BPM (beam propagation method) are methods belonging to this category. For the simulation of the optical properties of the LCD pixel, it is generally sufficient to consider the polarisation vector and its spatial variation over the domain. The transmitted intensity is then determined from the polarisation vector of the light and the initial intensity. A class of methods, such as the Jones' method, extended Jones' method and Berreman's method commonly referred to as *matrix-based methods* are commonly used to model optical transmission of an LCD.

1.2 Objectives of the Thesis

Our primary aim has been to evolve an open source code capable of simulating the dynamic and electro-optic behaviour of the pixels. Towards this broad aim, the objectives of this thesis include:

- **To evolve a nematic dynamics simulation method using appropriate theory**- We have used the Landau-de Gennes Q tensor theory for the LC phase simulations. The details of this theory are included in the Theory chapter.
- **To perform a parametric analysis based upon a modern pixel configuration to look at how changes in the applied voltage, the pixel depth, the electrode spacing and the electrode width affect the deformation in the domain.**- Metrics were evolved to compare the twist and tilt of the LC domain for a modern LCD configuration - the in-plane switching (IPS) mode.

The thesis is organised into seven chapters. :

- The second chapter contains an introduction to the history of LCDs, a brief overview of the various different liquid crystalline phases and a brief discussion on numerical simulations of the LCD domain.
- The third chapter contains an overview of the continuum theories for the nematic liquid crystalline phases.
- A review of the existing literature in this field is included in the fourth chapter
- The fifth and the sixth chapters discuss the results.
- The conclusions of the work and also the envisaged future directions of the project are covered in the seventh and final chapter.

Chapter 2

Background

2.1 Liquid Crystalline Mesophases

Liquid crystals form an interim state of matter between crystalline solids and isotropic liquids as shown in fig. 2.1. They have physical properties similar to isotropic liquids, but, in general show more order than normal isotropic liquids. Both liquid crystals and crystalline solids are optically anisotropic. Anisotropy arises on account of the increased ordering of constituent units in such molecules. Isotropic liquids generally do not show any orientational or positional order while liquid crystalline molecules shows varying degrees of orientational and/or positional order. For instance, the nematic phase shows no positional ordering, but a preferred tendency to point towards a particular direction, generally labelled as the *director* **n**. However, it must be noted that the director only shows the average orientation of the molecules in the liquid crystalline phase and the orientations of individual molecules may vary widely for a given ensemble. In the absence of biaxiality, the degree of ordering is represented by a scalar order parameter **S** defined as [23]:

$$S = \frac{1}{2}\langle 3\cos^2\theta - 1\rangle \tag{2.1}$$

where θ is the angle between the long axis of a particular molecule and the director. The angle brackets generally denote an average over time or an ensemble average of a sample at a particular instant of time. Thus, in an idealised scenario of perfect ordering, all the molecules would be aligned along the director n, and thus, S would assume the value 1. Conversely, on the other end of the spectrum, for an ideally disordered state, S would be equal to 0. Thus, 0 and 1 are the theoretical limits for the value of S. It may be noted that

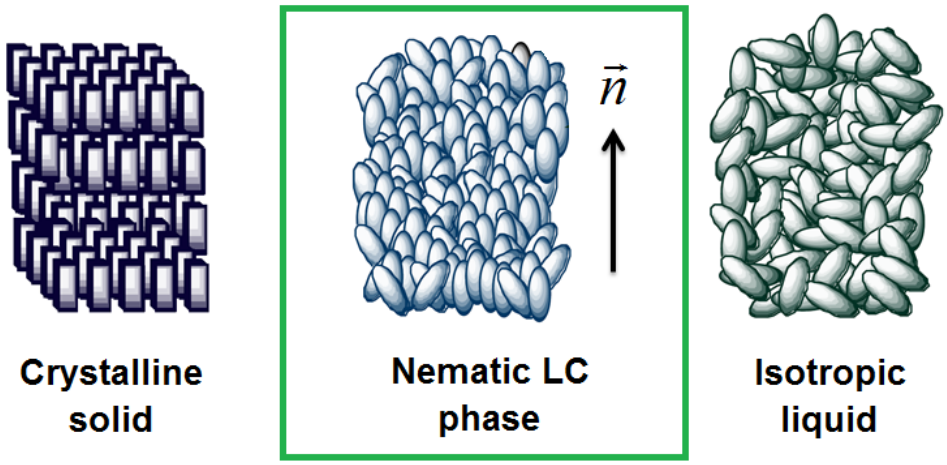

Figure 2.1: Schematic of a crystalline solid, nematic LC and isotropic liquid. The differences in the positional and orientational ordering of the three phases- solid, liquid and liquid crystal can be seen in the figure. The LC phase depicted here is more similar to the nematic phase and does not exhibit positional ordering [2].

isotropic liquids have a value of S that is equal to 0 as they are considered to be perfectly disordered.

Liquid crystals may also be classified depending upon the shape of individual LC molecules. *Calamitic* or rod-shaped molecules are the most common. These molecules may have a rigid central core (made of aromatic rings) and flexible ends (made of aliphatic chains). Disk-shaped molecules generally containing a number of rigid aromatic rings at the centre and surrounded by rigid aliphatic chains may also form liquid crystalline phases. They are referred to as *discotic* LC materials. Both calamitic and discotic materials can show various LC phases depending upon the degree of ordering. For instance, calamitic liquid crystals may form nematic and smectic phases while discotic molecules may form nematic or columnar mesophases.

As pointed out earlier, both calamitic and discotic LC molecules may form a number of different LC phases having varying degrees of order. For most LCDs, only the *nematic* phase is relevant. Molecules in this phase only show a varying degree of orientational order and no positional order. Orientational order manifests itself as preferential orientation along the director as discussed earlier.

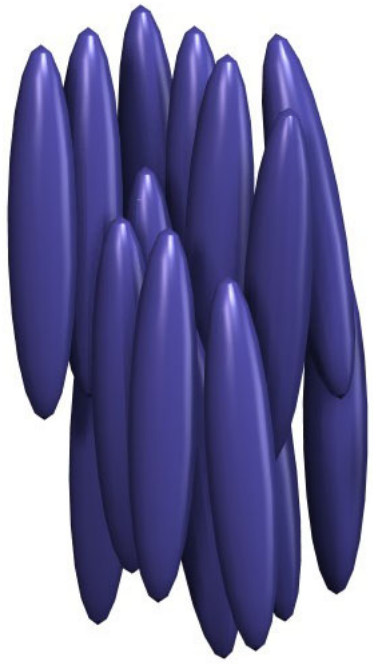

Figure 2.2: Schematic of a calamitic liquid crystal molecule in the nematic phase. The shape of the molecule is elongated. Molecules of this type are generally rigid at the center with one or more aromatic rings and flexible at the edges with aliphatic chains [3].

2.2 Development of LCDs

The first functioning mode of an LCD was the *guest-host* mode in 1964. A pleochroic dye having different optical properties in different directions acted as the *guest* phase, while the liquid crystal molecule acted as the *host* phase. Upon actuation by an electric field, the host molecules re-align themselves and change the optical properties of the associated guest phases. [20]

The first electronic devices to use LCDs were electronic watches and calculators. These devices required a display for relatively static images and limited variation in the grayscale. The dynamic scattering mode (DSM) was used in these early devices. It was based on the principle that in a randomly oriented LC domain, the transmitted light gets scattered randomly making it opaque. Upon actuation, the LC domain attains a striped appearance (*Williams domains*) followed by a turbulent appearance at higher voltages which resulted in light being scattered away (*electro-hydrodynamic instability*). The LC material often

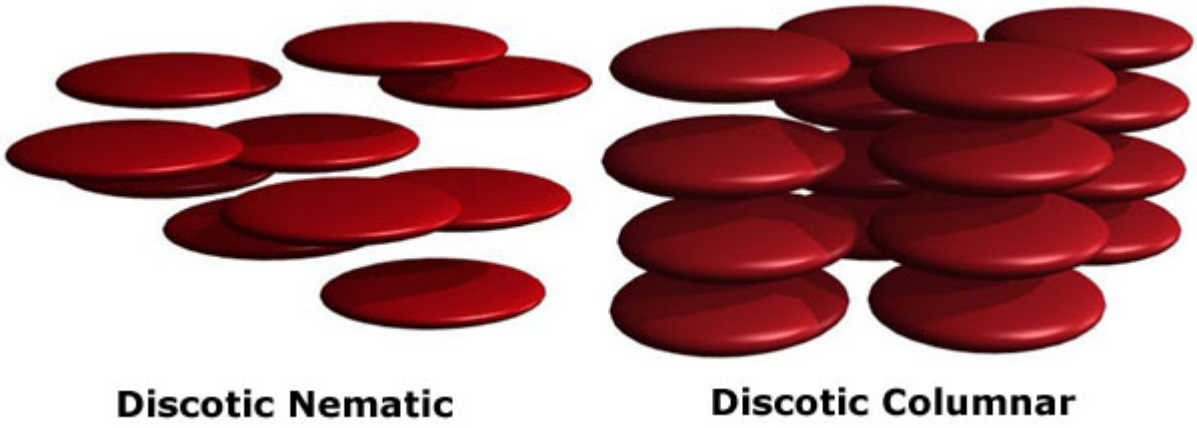

Figure 2.3: Schematic of a discotic liquid crystalline molecule. Molecules of this type generally have one or more rigid aromatic cores and a number of aliphatic chains at the ends that gives the whole molecule a disk-like appearance [4].

had to be doped to increase its conductivity and the continuous flow of electric current had to be ensured to make the domain appear cloudy. The flow patterns indicate that the optical effects arose on account of the dynamic motion in the LC phase [20].

Application of LCDs to large television screens and computers had to await the development of the twisted nematic (TN) mode by Schadt and Helfrich in Switzerland [24]. The TN and most subsequent modes have concentrated on modifying the polarisation state of the transmitted light. The TN had an LC domain twisted uniformly by an angle of $\frac{\pi}{2}$ radians over the domain sandwiched between two crossed polarisers. In the OFF state, the polarisation vector of light followed the twist of the domain due to wave-guiding and light could pass through the second polariser, However, in the ON state, the twist in the domain was broken and the polarisation vector of transmitted light could not align itself to the second polariser and thereby was blocked.

Despite its advantages, the TN mode and its later modifications such as the STN (super-twisted nematic) mode had an important drawback: they had a very narrow viewing angle [25]. Off-axis image quality deteriorated substantially for these modes of operation. This is due to the fact that away from the optical axis, the LC domain loses its birefringence and only an optically uniform domain is presented to the light. Wave-guiding cannot take place in the absence of birefringence and thus, the optical properties of the pixel degraded sharply in such regions.

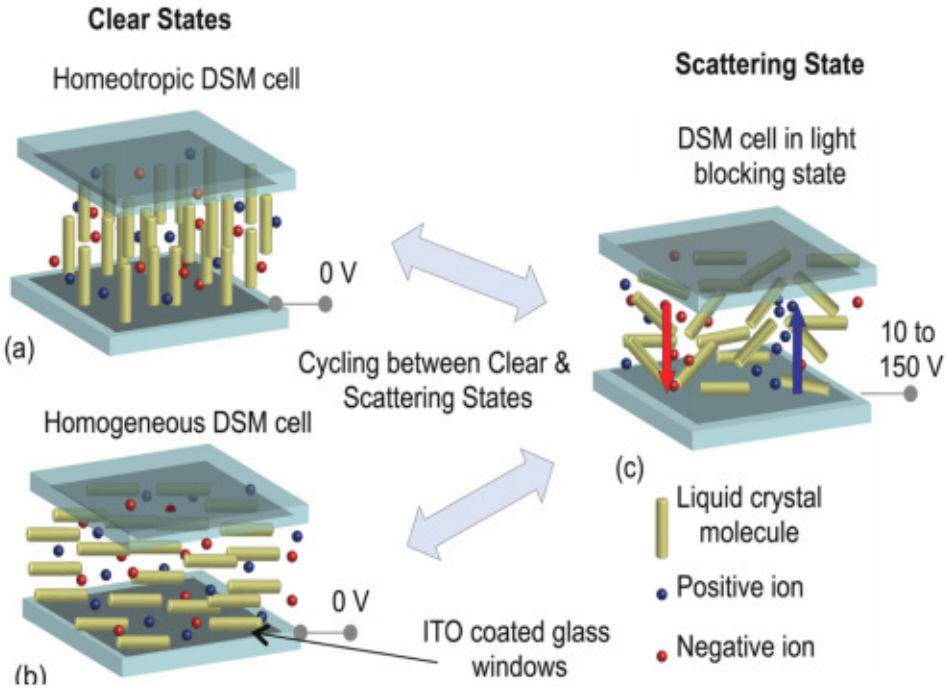

Figure 2.4: A schematic of the dynamic scattering mode of a liquid crystalline based light shutter. The schematic is very similar to what was intially used in dsm based lcd pixels. The above figure gives two clear states and one translucent/opaque state in the ON state [5].

IPS mode was first developed in the 1990s [26]. It consists of interdigitated (finger-like) electrodes on only one end of the domain. The electric field in the domain is highly inhomogeneous and consists of alternate regions having either predominant *twist* or predominant *tilt*. The terms *twist* and *tilt* refer to re-orientation predominantly along the horizontal axis or along the vertical axis. As most liquid crystalline materials used in LCDs are of the p-type ($\varepsilon_{||} > \varepsilon_{\perp}$), the induced reorientation of the LC phase aligns the domain in the direction of the electric field. Thus,the parallel component of the electric field (mainly in regions between electrodes) induces an in-plane twist in the LC domain while the vertical component(in regions directly above the electrodes) induces a vertical tilt.

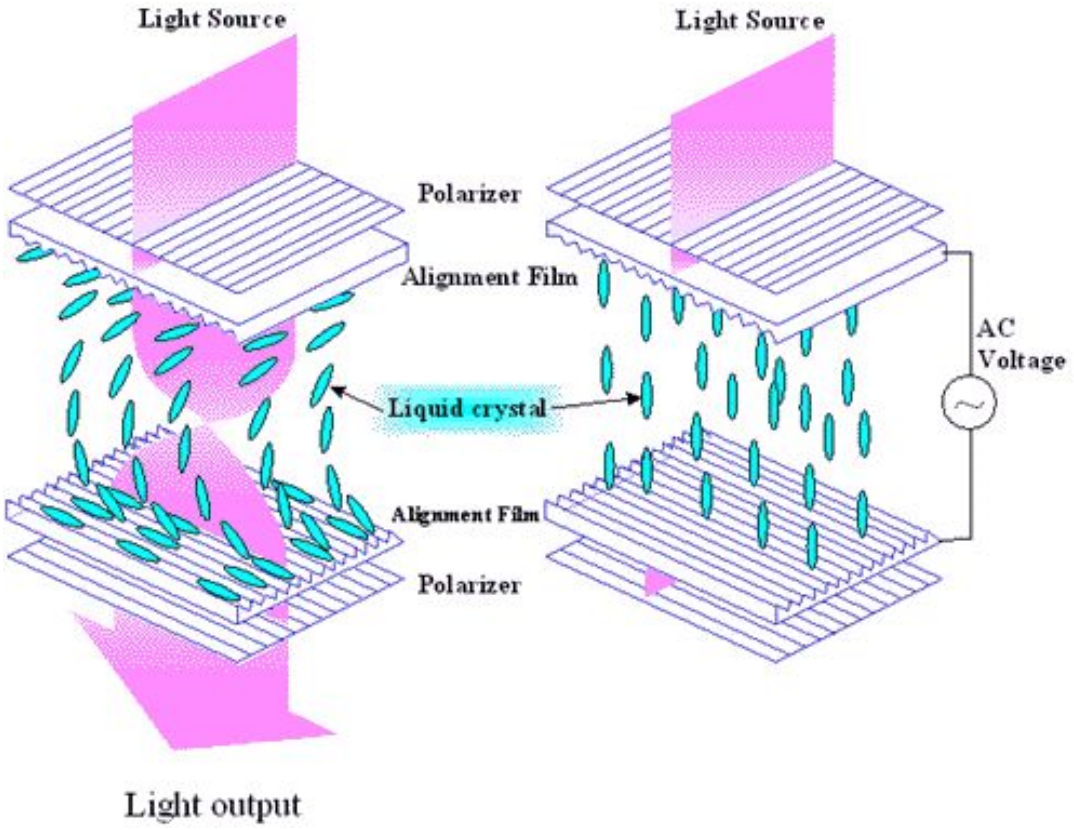

Figure 2.5: A schematic of the twisted nematic(TN) mode of a liquid crystalline based light shutter. The schematic shows the pixels in both the OFF state (left) and the ON state (right) [6].

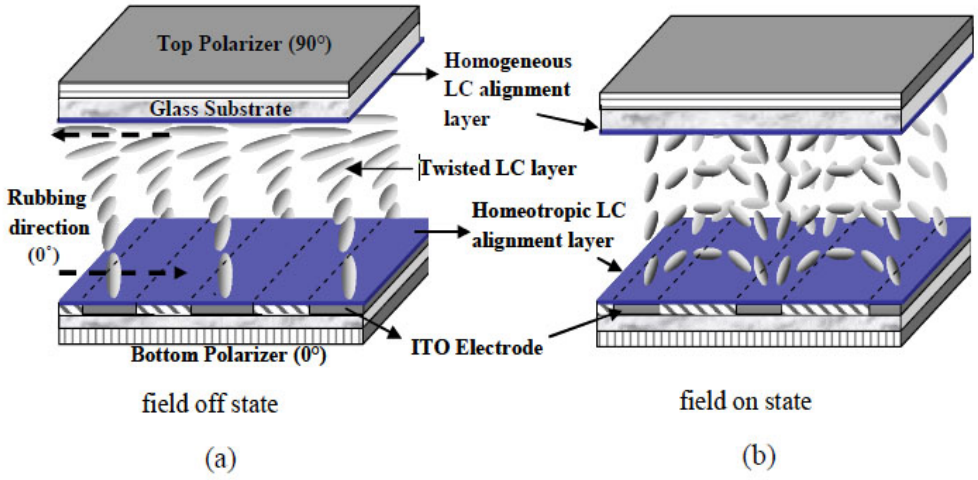

Figure 2.6: Schematic of in-plane switching mode(IPS) of LCDs. The figure shows the electric field patterns and the associated re-alignments of molecules in response to the electric field. The liquid crystalline molecules in the figure can be seen to rotate in the in-plane direction, (a) shows the OFF state that does not allow light to pass through while (b) shows the ON state that transmits light [7].

2.3 Liquid Crystal Display: Operating Principles

Being an electromagnetic wave, light is composed of electrical and magnetic waves that are mutually orthogonally and also orthogonal to the direction of propagation. By convention, the vector representing the direction of oscillation of the electrical wave is taken to be the polarisation vector for the light. For a transverse wave, the polarisation vector can be considered to be made up of two independent and orthogonal components. If no correlation exists between these two components, then the light is said to be unpolarised [27].

For polarised light, the phase difference between the two components of the polarised light is well defined. Elliptically polarised light, the most generalised case, occurs when the two waves have unequal amplitudes and a phase difference other than 0 or π. The resultant polarisation vector traces out an ellipse as the light propagates in space. It may be noted that the principal axes of the ellipse might not align with the coordinate axes used to define the orthogonal components of the light.

Circularly polarised light occurs when the interacting plane waves have equal amplitudes and are $\frac{\pi}{2}$ out of phase with each other. The polarisation vector of the resulting

beam, traces out a circle in the plane of oscillation. Linearly polarised light, on the other hand, occurs when the interacting waves are exactly in phase or π out of phase. In this case, the polarisation vector is constant and has a particular direction.

Being polarised parallel and perpendicular to the optic axis of the LC, for a general case the two waves in a uniaxial nematic interact to yield elliptically polarised light. For particular values of the phase difference, the resultant polarisation is linear or circular, in which case the resultant light beam can be extinguished by an appropriately oriented analyser placed at the viewer side of the domain.

For particular orientation of the linearly polarised light beam at the entrance and small rates of twist over the domain, the phenomena of *waveguiding* is experienced. In this case, the orientation of the resultant light beam follows the director of the LC domain as it propagates through the domain.

The dielectric anisotropy of a nematic liquid crystal is given by a second order tensor composed of two scalar constants, $\varepsilon_{||}$ and $\varepsilon_{\perp}$. These constants are directly related to the refractive indices of the liquid crystal n_e and n_o parallel and perpendicular to the director of the LC, respectively. Thus, a linearly polarised light polarised in any direction other than the optic axis, splits up into two mutually orthogonal waves upon passing through such a media. The component parallel to the optic axis is called the *extraordinary* component while the component orthogonal to the optic axis is called the *ordinary* component. These two mutually orthogonal waves propagate through the media with different phase velocities and the relative phase difference between these two components continuously changes as they pass through the media. The effective refractive index for the extraordinary wave is given by [27]:

$$n = \left(\frac{n_e^2 \cdot n_o^2}{n_e^2 \cos^2 \theta + n_o^2 \sin^2 \theta} \right)^{\frac{1}{2}} \tag{2.2}$$

Most LCDs are designed to operate in the waveguiding regime so as to manipulate the orientation of the polarisation vector of the emergent light beam directly by controlling the orientation of the LC domain. The transmissivity of the LCD pixel depends on the orientation between the optic axis of the second polariser and the direction of polarisation of the light beam.

Modern liquid crystalline display pixels thus work as polarisation state modifiers of the input light beam and effectively act as phase retardation plates. Intensity of light transmitted is thus manipulated by changing the polarisation state of the light beam propagating through the medium. The dark state of the pixel, thus, often depends on the viewing angle. At larger viewing angles, the apparent orientation of the light beam with respect to the

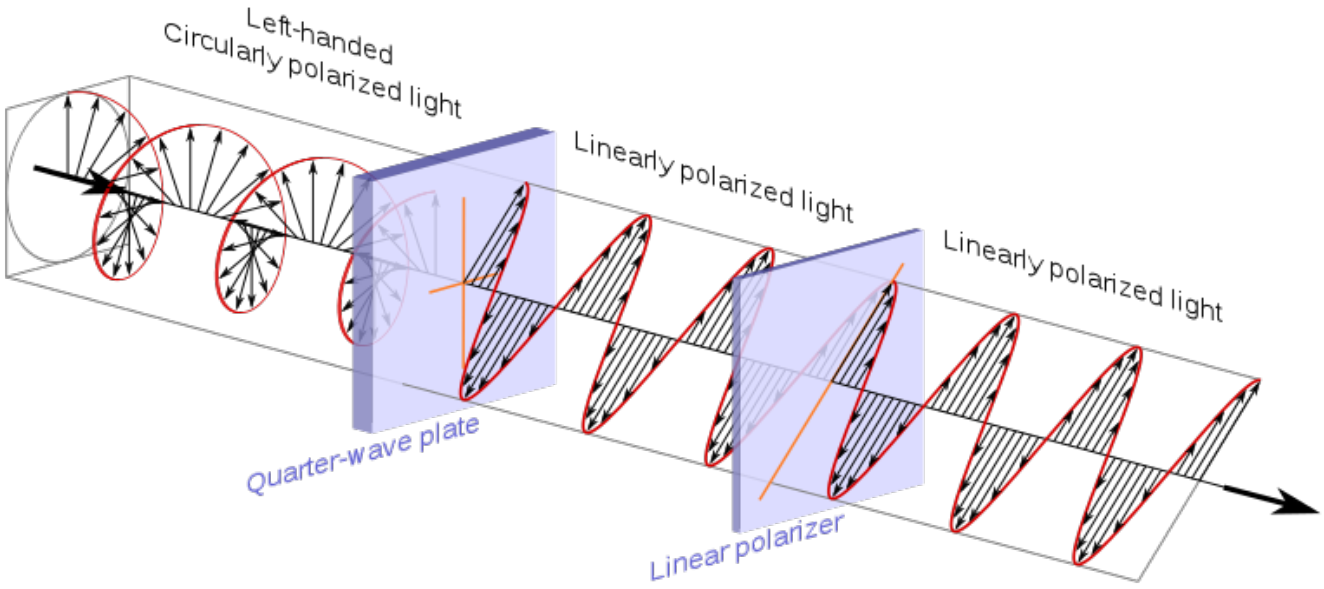

Figure 2.7: An image of circular polarised light getting converted to linearly polarised light after passing through a retardation plate. Conventionally, the direction of vibration of the electric field vector is taken to be the direction of polarisation of an electromagnetic wave. In the general case, light is elliptically polarised and linear or circular polarisations are seen to occur only at specific values of the relative phase difference [8].

second polariser might not cause full extinction and this results in the phenomenon of light leakage that is often observed in many LCD pixels. Furthermore, thus results in a finite contrast ratio (CR) for LCD pixels. Active display devices such as OLEDs theoretically have an infinite contrast ratio as in those modes, the display might simply be turned off to creates the dark state.

The in plane switching(IPS) mode of operation of LCDs consists of a layer of nematic material sandwiched between crossed polarisers and glass substrates. The electric field for actuation of the liquid crystalline domain is applied by means of interdigitated electrodes on only one side of the domain. The electric field that is applied thus varies both parallel to the substrate as well as decreasing exponentially vertically through the domain.

Liquid crystalline materials normally used in such displays are p-type, where $\varepsilon_{||} - \varepsilon_{\perp} > 0$. Thus, upon application of the electric field, the LC molecules align parallel to the electric field. As the electric field has both in-plane and through-plane components, LC molecules

in different regions of the domain align either in the in-plane or the through-plane direction upon application of the electric field creating different regions of tilt and twist.

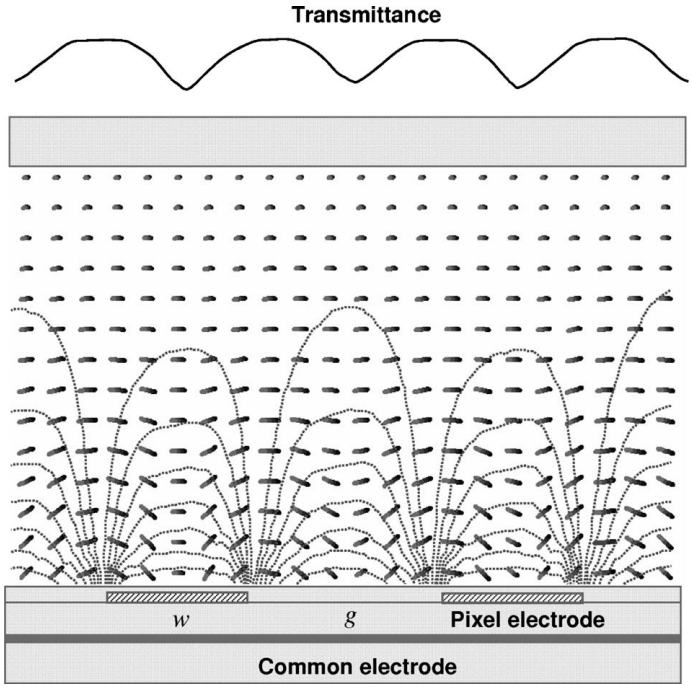

Figure 2.8: Transmittance and director profiles of an FFS cell. The FFS and the IPS cells are very similar and both exhibit alternate regions of twist (in-plane alignment) or tilt(through-plane alignment). The transmissivity is high for regions showing high twist and lower for regions of high tilt [9].

Thus, in a nutshell, IPS technology works by creating an induced twist in the LC domain upon application of the electric field. The phenomenon of wave-guiding of the initially polarised light makes the polarisation vector of light follow the twist of the domain. As the domain consists of alternate regions characterised by twist and tilt, the transmissivity of the domain varies across the domain, being higher for regions with higher twist.

The fringe field switching(FFS) mode differs from the IPS mode in terms of its electrode structure, but has a similar working principle. The aperture ratio characteristics of the FFS mode are slightly better than those of the IPS mode [28]. The electric field distribution patterns and the deformation of the LC domain are similar to that in an IPS cell.

Chapter 3

Literature Review

The story of the development of liquid crystal displays, from the identification of liquid crystalline phases in the late 19^{th} century to the development of the Twisted Nematic mode of LCD operation is reviewed in details in ref. [20]. In the following paragraphs, we give an outline of some of the developments in the field from the 1990s to the present. It is worthwhile to point out that the IPS mode of LCDs was first developed in the 1990s.

3.1 Numerical Modelling of LCD devices: An Overview of Previous Studies

Most approaches for modelling the dynamics and the electro-optical performance of liquid crystal displays follow a standard approach. The first step involves modelling the deformation of the LC phase by electric field using models such as the Landau-de Gennes Q tensor theory [29] or the more popular Frank-Oseen director deformation theory [30]. The Ericksen-Leslie theory [29] has also been used to model the deformation of the LC phase.

The next step involves simulating the optics. Approaches developed for the propagation of light in stratified media such as the Jones' matrix method have been shown to be quite effective in modelling the optics of the LC domain. Methods are divided into two main classes: matrix-based methods (Jones method [31], extended Jones method [32], Berreman's method [33], etc.) or methods based on full scale simulations and numerical solutions of Maxwell's equations(Finite Difference Time Domain(FDTD) [34], Beam Propagation Method(BPM) [35],etc).

In general, matrix-based methods are sufficiently accurate for purposes of simulating the optics of LC displays. Most commercial software packages and published work use either the extended Jones matrix method or the Berreman's 4×4 matrix method for modelling the optics.

Continuum models of the liquid crystalline phase make use of the expression of the Helmholtz free energy of the liquid crystalline phase. The Helmholtz free energy is generally expressed as a functional of some quantity that is characteristic of the deformation of the LC phase. The free energy functional can be minimised using calculus of variations to yield the equilibrium configuration of the LC domain. The Oseen-Frank director theory and the Landau de Gennes Q tensor theory are the two most commonly used models of the continuum phase of nematic liquid crystals.

Although more popular, the Oseen Frank theory, makes the approximation that only elastic forces contribute to the free energy density of the nematic phase. This approximation may be questioned in the bulk of the LC domain far away from boundaries and also near the points of phase transition. The Landau-de Gennes Q tensor theory, on the other hand, estimates that the free energy is a combination of both thermodynamic terms and elastic terms. Thus, the approximation is more realistic and accurate, especially at points of phase transition. On the other hand, the Oseen Frank theory is vectorial in nature and thus more amenable to numerical methods.

The finite element method (FEM) is popular amongst researchers working on the modelling of LCDs. Ge *et al.* in [10] point out several advantages of FEM over other computational techniques such as its ability to handle complex and arbitrary geometries. Furthermore, evolution of symbolic computation software packages have considerably simplified the derivation of weak form equivalent formulae for finite element formulations.

The suitability of the finite element method for the modelling of the LC dynamics can be demonstrated by the fact that this is the approach used in several commercial LC modelling software packages such as dimMOS [36] and Techwiz LCD 3D [37] in combination with finite difference methods to model LC deformations.

A major drawback of the TN mode display was the poor off-axis image quality. These problems were recognised early on and efforts to improve the viewing angle characteristics included approaches such as the use of multiple domains in the twist cell, the use of optical compensation films and the use of different configurations of the LC domain such IPS, fringe field switching (FFS) and vertical alignment (VA).

The TN mode is sometimes made to operate in the normally white (NW) mode, which simply refers to the fact that it allows light to pass through in the absence of applied electrical field while blocking it when electric field is switched off. In the OFF state, the

molecules are tilted along the vertical direction, thus, light travels parallel to the optic axis and does not experience any birefringence. However, when viewed at larger viewing angles, the light sees a certain amount of birefringence and thus, undergoes wave-guiding. This creates light leakage at larger viewing angles as some of the light passes through the domain on account of the wave-guiding phenomena.

Use of a multi-domain configuration, wherein the pixel is sub-divided into a number of sub-domains improves the viewing angle characteristics by ensuring a more random distribution of orientations in the LC domain. This ensures that the overall birefringence does not vary much spatially throughout the domain. In ref. [38], for example, the authors use a four-domain configuration to give better viewing angle characteristics and improved off-axis image quality.

Use of optical compensation films has also been popular as pointed out [27]. This works by ensuring that the positive retardation imparted to the off-axis light by the LC domain in the ON state is nullified to some degree by a negative c-plate. A c-plate is one where the c-axis is along the direction of propagation of light. It is worthwhile to note here that TN LCD pixels normally employ an optically p-type liquid crystal. Smectic liquid crystals have also been used as optical compensation films [39] for a similar purpose.

The development of display configurations such as the IPS in the 1990s signalled a new era in LCD display technology. Prior to that time, LCDs held the market in small sized information display systems, but were considered to be unsuitable for larger displays. Technology such as the IPS mode allowed LCD technology to compete with other modes such as OLEDs (organic light emitting diodes), PDPs (plasma display panels) and CRTs (cathode ray tubes). The latter would soon become obsolete. A very good account of developments in that decade is given in [40].

An example of some of the earlier approaches towards computational studies on the IPS LCD pixel is given in ref. [26] . In this paper, the authors examined the switching behaviour of the pixel. Dirichlet boundary conditions, physically corresponding to strong anchoring at the boundaries was assumed to prevail. The authors also derived an expression for the threshold voltage of this particular configuration. Unlike the TN mode of LCDs, the IPS mode has a non-uniform electric field over the LC domain and the threshold voltage would depends on the inter-electrode distance in the IPS mode. It was also determined that the threshold voltage depends on the cell gap.

Due to the complex electric field in the IPS configuration, 1D simulations of the pixel domain are insufficient. At the very least, simulations in 2 dimensions are required. In [41], the authors present a finite element-based code for modelling the LC domain in 2 dimensions. The authors used the Oseen-Frank's director theory for continuum phase

modelling of the LC domain and assumed strong anchoring conditions at the boundary. The final form of the Euler-Lagrange equation minimising the free energy was non-linear and also involved coupled terms of the director field and the electric field in the domain. The authors used an iterative approach wherein the electric field was first calculated for a known director field and then the obtained electric field was used to determine the reorientation of the LC molecules in the domain. The process was continued until convergence was reached.

In [42], the authors investigated the dynamic response times of the IPS LCD domain. They used a simplified form of the Ericksen-Leslie equation to model the LC dynamics. Both the switch on and the switch off response behaviour were modelled and factors on which the rise time and the decay time depend were determined. Apart from the obvious choices of a low viscosity and a high elasticity, a thinner cell gap was also considered to be beneficial as it led to an increase in the effective elastic force. The electrode spacing was not found to exert a big influence as the electric field affects the reorientation of the LC molecules and not the applied voltage between electrodes. In other words, as the electrodes are present on only one side of the domain, other factors in addition to the applied voltage between electrodes affect the final electric field responsible for switching of the LC molecules.

Although most papers use Frank-Oseen director theory to model LC deformation, the Q tensor theory has also been used [43]. Although, the authors only used the Q tensor theory to model the elastic deformation part of the total free energy and seemed to overlook the temperature dependent contributions to the free energy, they considered various methods to simulate the domain and ultimately ended up using a relaxation method. A SOR method was used to model the electric field distribution in the substrates and the LC material. Boundary conditions for the electric field were based on the assumption that the field decays to zero at infinite distance from the electrodes. This method involved simultaneously solving both the electric field distribution and the director distribution which led to faster convergence than the iteration-based method. The authors also compared results between the tensor method and the director method. If adjacent director fields differ by less than $\frac{\pi}{2}$ radians, the results were found to be similar, while the Q tensor theory gives a lower free energy for greater values of the angle. The simulation results were applied to a π cell (a type of LC cell) and the results were compared to experimental observations to give good agreement.

In [44], the authors used two different methods of discretisation: the finite element method and the finite difference method and compared the results for an IPS cell in terms of CPU time. For the FEM-based formulation, the Ericksen-Leslie equations were formulated in bulk using a Galerkin-FEM method. A Rapini-Papoular type of expression was used to express the surface energy. The electric field was calculated by solving Gauss's law

and the Ritz method was used for the resulting Laplace equation. On the other hand, a 3-dimensional centred finite difference formulation was used for the finite difference-based algorithm. It was reported that the finite difference method was slightly faster than the finite element method.

In [45], the authors used a 3 dimensional finite element-based method to simulate the dynamic behaviour and electro-optic response of a liquid crystalline domain in the IPS configuration. The simulations revealed that the in-plane re-orientation of the LC molecules occurs first despite the electric field varying spatially and the existence of both horizontal and vertical electric fields. The Ericksen-Leslie equation is used to model the dynamics and the bulk free energy term is given by the Frank-Oseen formulation. The electric field gets coupled to the director field in the final equation. This term is handled by using an iterative method for simulations in which the Laplace equation (for electric field) is solved using an assumed director configuration and then the director configuration is solved for this particular electric field. Strong anchoring at the interfaces was assumed. The magnitude of the electric field between electrodes was calculated to be about 3.5×10^6V/m, whereas the other regions have lower electric fields of about 10^5V/m. Cell capacitance was found to saturate at times less than 10 ms and thereafter, the director orientation was influenced solely by the orientations of the directors in surrounding molecules and not solely by the electric field. Thus, the electric field re-orients the directors in the regions close to the electrodes and then these molecules cause the others to re-orient.

In [46], the authors examined techniques to calculate the electric field in the IPS domain and then used these to calculate the threshold voltage and also the parametric dependence of the threshold voltage on various parameters.

In [10], the authors used the Oseen-Frank theory to model the deformation of the LC director profile. This form led to coupled equations for the director field and the voltage in the domain. An iterative technique was adopted wherein the relevant PDEs were solved in successive steps to give the voltage and the director field.

The authors used Galerkin's FEM method to solve the Euler Lagrange equation to minimise the free energy of the LC phase. The weak form of the equations was used to approximate the equations involving the volumetric integrals. The total free energy was assumed to be obtained by the volumetric integral of the free energy density given by the Oseen Frank theory. A finite difference scheme was used to step through time.

The potential profile was obtained by solving Gauss's law. The authors used Ritz's method to solve for the second PDE. A successive iteration scheme was used to solve for the coupled set of PDEs. The authors compared the results obtained by their code to those using the commercial software 2-dimMOS for a 2-dimensional IPS configuration.

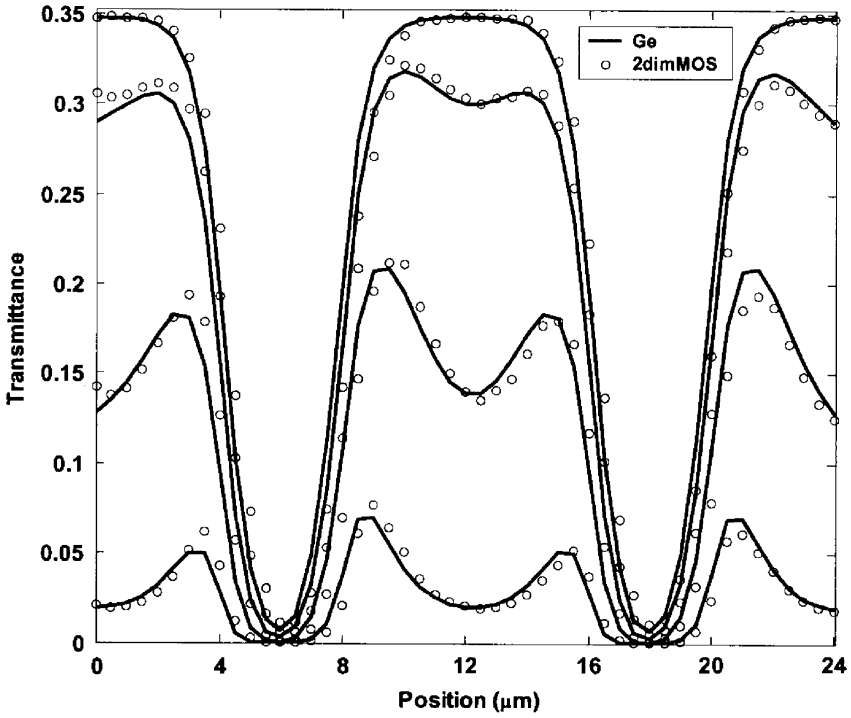

Figure 3.1: Transmittance profile of method proposed by Ge *et al.* and predicted by commercial software 2dimMOS. The alternate crest and trough pattern is characteristic of IPS and FFS type of devices having alternate regions of high twist and high tilt [10] ©2005, IEEE

.

The FEM-based method proposed by the authors showed a very good correlation to results given by the commercial code 2-dimMOS for the 2-dimensional IPS configuration. Good agreement of results with that produced using a commercial code in both cases was seen apart from regions of discontinuity.

A similar procedure as above was used in [11] to model the effect of the bending angle of the chevron-shaped electrodes which are characteristics of a Super-IPS display assembly. After modelling the director deformation, the extended Jones matrix method was used to determine the optical transmittance of the pixel assembly. The bending angle between the electrodes was varied between 10° and 45° for purposes of this analysis. The director distribution adjacent to the two arms of the chevron electrode showed switching in the complementary directions, thus, giving rise to a four-domain structure. As in conventional

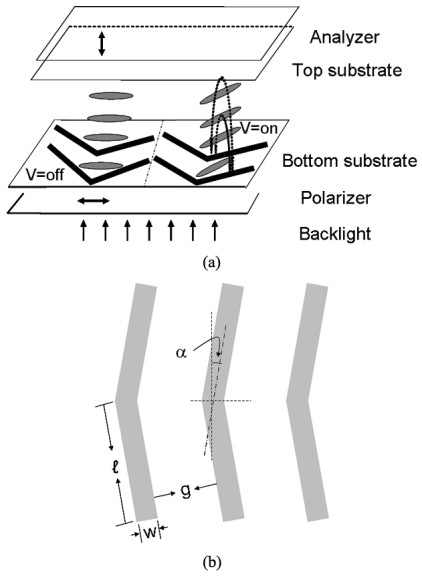

Figure 3.2: The chevron-shaped electrodes of a super-IPS LCD assembly. The bending angle, α refers to the angle between the arms of the chevron and the vertical axis [11] ©2005, IEEE.

IPS electrodes, the regions directly above the electrode exhibited a very low transmittance and thus formed dead zones, reducing the overall intensity.

The transmittance was studied for three different wavelengths: red (650 nm), green (550 nm) and blue (450 nm). The threshold voltage was found to be about $1.2V_{rms}$ and the voltage for maximum transmission occurs occurred at about $5V_{rms}$. It was also observed that the voltage for which maximum transmission increased with a rise in the bending angles, although, the value of the maximum transmittance itself decreased with an increase in the bending angle. The increase of bending angles also led to shorter rise times due to an increase in the effective applied voltage and a lower threshold voltage, but the decay time remained largely unaffected. The bending angles are the angle between the arms of the chevron-electrode and the vertical direction.

LCDs are passive displays, meaning that they merely manipulate light passing through them and do not produce their own light. LCD panels often consist of a backlight panel which actually produces the light. Conventionally, backlight panels are of the CCFL (cold cathode fluorescent lamp) type. However, LED (light emitting diode) panels are being increasingly used in backlight panels.

In a separate paper [12], the authors also used a very similar procedure to analyse

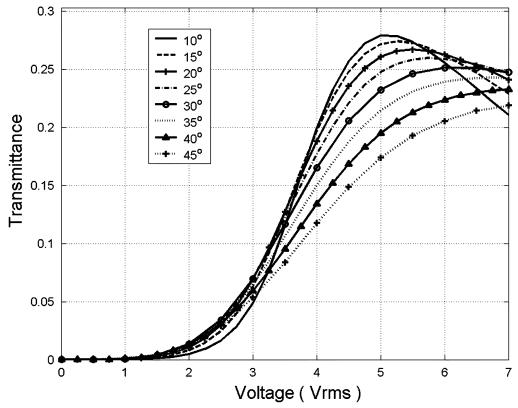

Figure 3.3: Variation of transmittance with bending angle in a multi-domain S-IPS configuration [11] ©2005, IEEE.

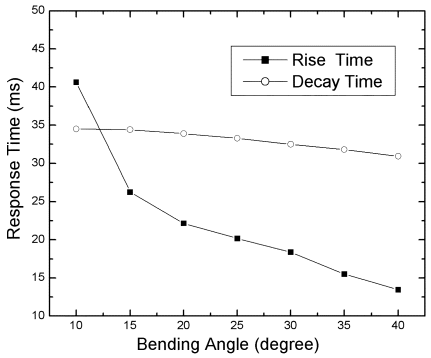

Figure 3.4: Variation of rise time and decay time with the bending angles [11] ©2005, IEEE.

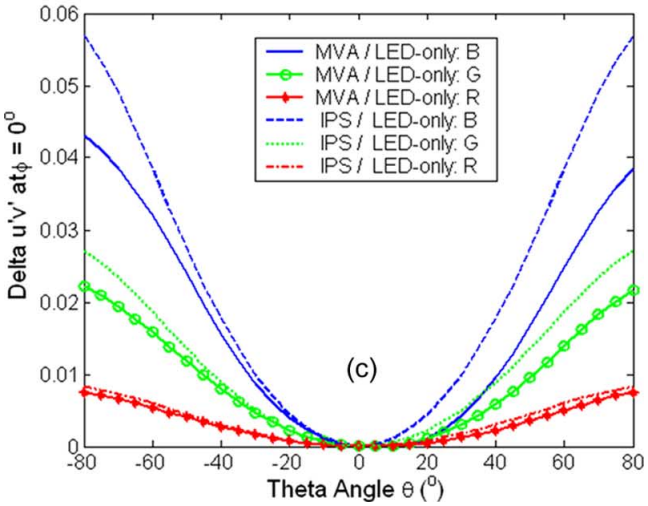

Figure 3.5: Color shift of an LCD having CCFL and LED backlights with color filters. [12]. ©2006, IEEE.

the color gamut and color shift of multi-domain IPS cells and MVA cells having CCFL (cold cathode fluorescent lamp) or LED (light emitting diode) or a combined backlighting. Simulations demonstrated that the LED backlights exhibit wider color gamut and less color shift than LCD pixels with CCFL backlights. The performance of LED backlights was considerably improved if color filters were eliminated and RGB LEDs used in their place.

Fernandez *et al.* in [47] also came up with a modified finite element formulation to simulate the director dynamics in an LCD pixel. They used a form of the Frank-Oseen theory to derive the relevant deformation equations. Frank's theory states that any mechanical deformation of the nematic phase can be expressed in terms of three fundamental deformations- *splay*, *twist* and *bend*. Each of these fundamental deformations have a characteristic elastic constant (K_{ij}) associated with them. In order to remove non-linearity and simplify the discretisation process, the approximation $K_{22} = K_{33}$ was made. A similar assumption has been made in the present study wherein all the elastic constants have been assumed to be equal ($K_{11} = K_{22} = K_{33}$). Strong anchoring conditions were assumed (Dirichlet boundary conditions) at the surfaces of the substrates and Neumann Boundary Conditions were assumed to hold at the lateral edges of the pixel. Simulations of an IPS pixel having strip electrodes were carried out to validate the algorithm and the spatial variation of the transmittance was obtained.

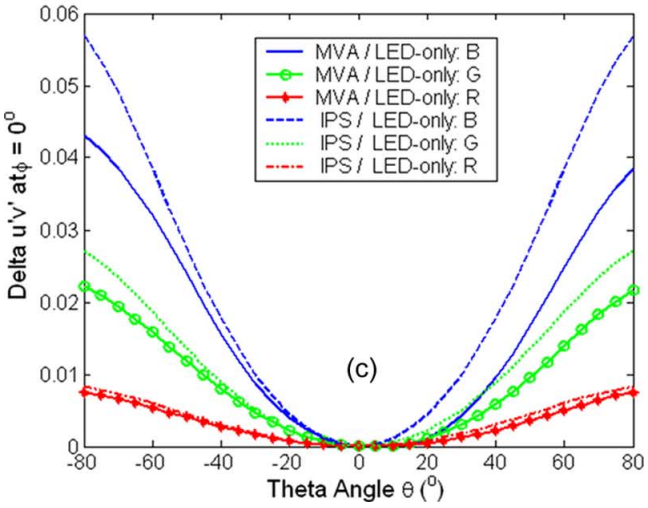

Figure 3.6: Color shift of LCD having RGB LED backlights [12]. ©2006, IEEE.

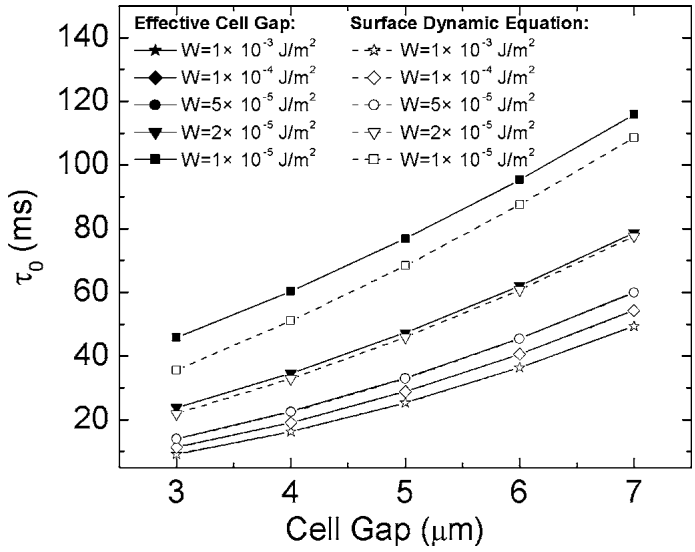

Figure 3.7: Decay time variation with cell depth [13].

Nie *et al.* [13] studied the effect of the cell gap and the anchoring conditions on the response times of the LCD pixels. They assumed that the response time of the LCD pixel is

given by adding the rise time and the decay time.The applied voltage has a strong influence on the rise time. The authors investigated the effect of the variation in the decay time with the cell gap by using two semi-analytical methods based on the extrapolation length and the surface dynamic equation. They also proposed a relatively simple dependence of the response time on the pixel depth ($t \propto d^x$, where d is the pixel depth) and fit their data to this equation. They found that $x \approx 1$ for weak anchoring and $x \approx 2$ for strong anchoring.

Wang *et al.* in [48] pointed out the distinction between the optical response time and the director reorientation time. An Ericksen-Leslie type formulation was used to model the dynamics of the LC domain in a vertically aligned configuration and the finite element method was used to numerically solve the associated PDEs. To model the optical response of the device, the authors used the extended Jones matrix method. The authors concluded that the optical response time was linearly proportional to the director reorientation time. Bias voltage was not found to exert a significant effect on the response times. However, the initial pre-tilt angle was found to affect the response times and the authors proposed the use of a modified rotational viscosity in the Ericksen-Leslie formulation to take this effect into account.

Park *et al.* in [14] proposed a new configuration called fringe in-plane switching (FIS). The electrode configuration is similar to the FFS mode, but unlike the FFS mode that only has negative interdigitated electrodes, the FIS mode has interdigitated electrodes with alternating polarity. The performance of the new mode was compared to the performances of the IPS and the FFS modes using a commercial LCD solver and the optics was simulated by means of the 2×2 extended Jones matrix method. Simulation results showed that the new mode of operation requires a much lower operating voltage than either of the conventional modes. FIS mode was shown to have higher transmittance than the conventional LCD modes of in-plane switching and the fringe field switching. Conoscopic studies demonstrated that the FIS mode exhibited the similar wide-viewing angle characteristic of the IPS and FFS modes.

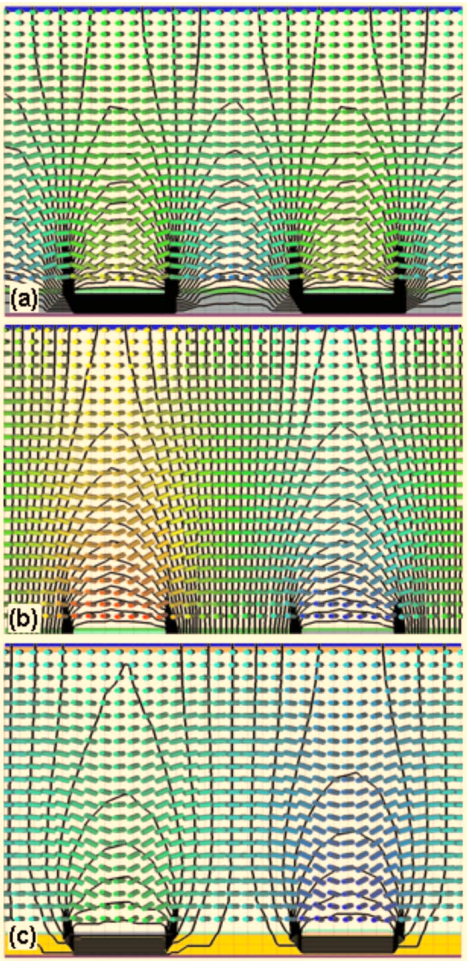

Figure 3.8: Electric field patterns and director distribution in the (a) FFS, (b) IPS and (c) FIS configurations. the black lines are equipotential lines [14].

Ge *et al.* in [15] proposed yet another minor modification to the design of conventional IPS cells to increase the overall transmittance. In this mode, called HT-IPS (high transmittance in-plane switching), regions of horizontal electric fields like in the IPS mode and fringe fields on top of electrodes were desired. The pixel electrodes were configured so that each common electrode formed an electrode group together with two pixel electrodes. Both the width of the pixel electrodes and the horizontal distance between the pixel and the common electrodes is smaller than the cell gap. The authors used a commercial package and the extended Jones matrix method for further simulations. The new mode showed

higher transmittance and a lower driving voltage than conventional modes of operation.

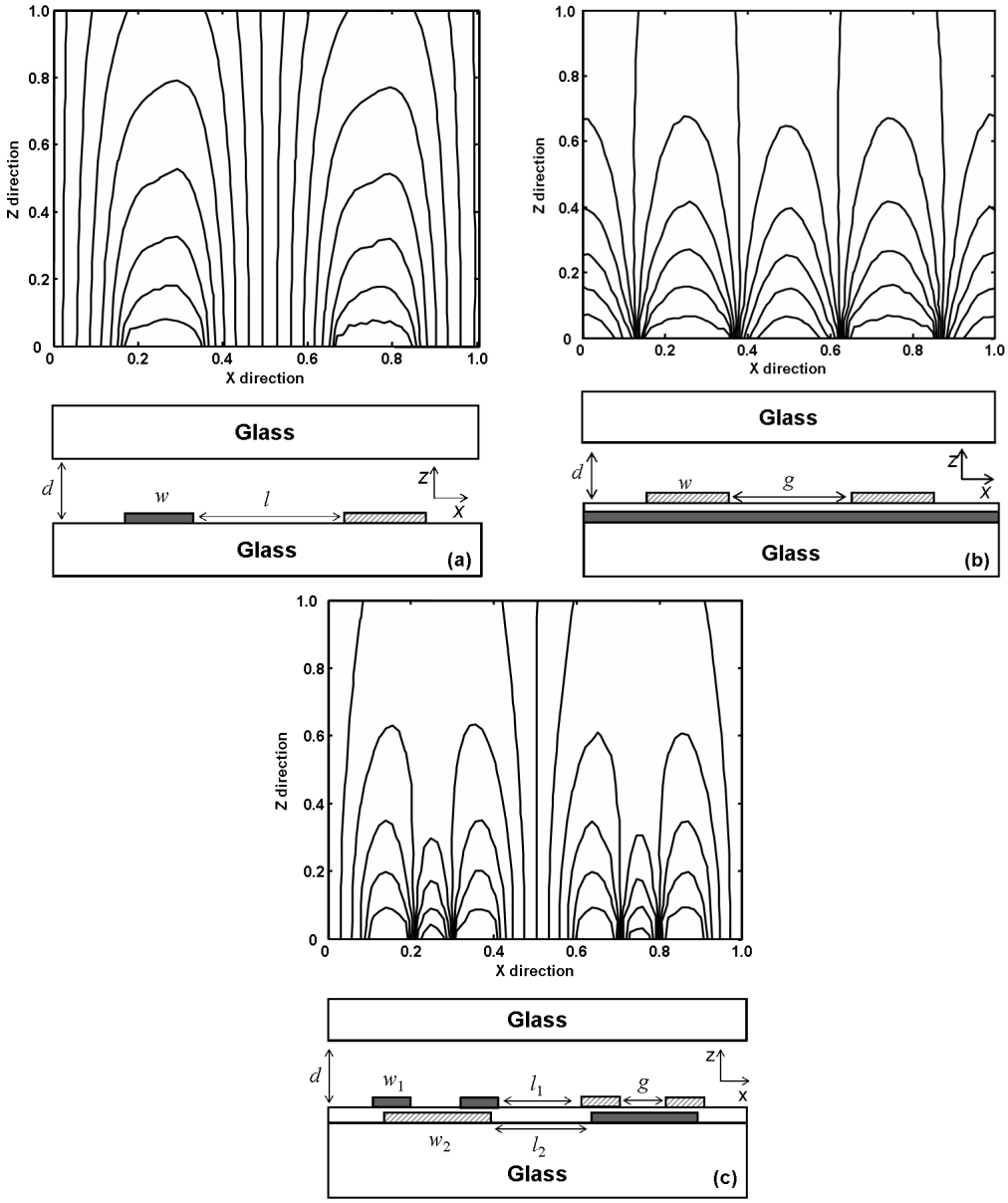

Figure 3.9: Structure and potential pattern of an IPS, FFS and the HT-IPS mode [15]. ©2006, IEEE.

Xu *et al.* in [16] pointed out several disadvantages of the conventional FFS pixel configuration such as a slow response time and image sticking. The authors proposed a new configuration called PCFFS using Patterned Common electrodes that shows better response time and electro-optical characteristics. In contrast to a conventional FFS configuration that has an non-patterned common electrode and interdigitated pixel electrodes, the proposed configuration has a patterned common electrode as well.

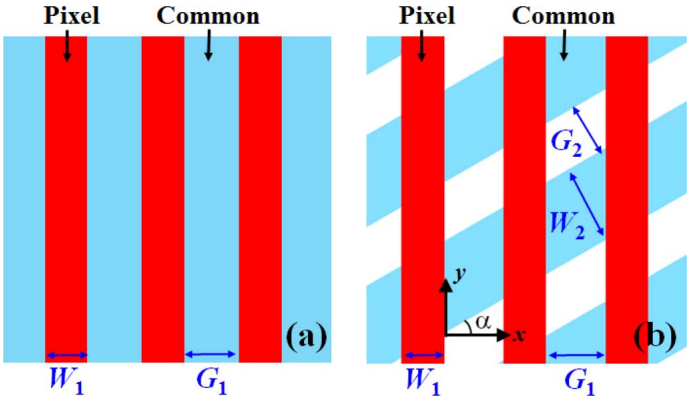

Figure 3.10: Schematic of an FFS device structure [16]. ©2015, IEEE.

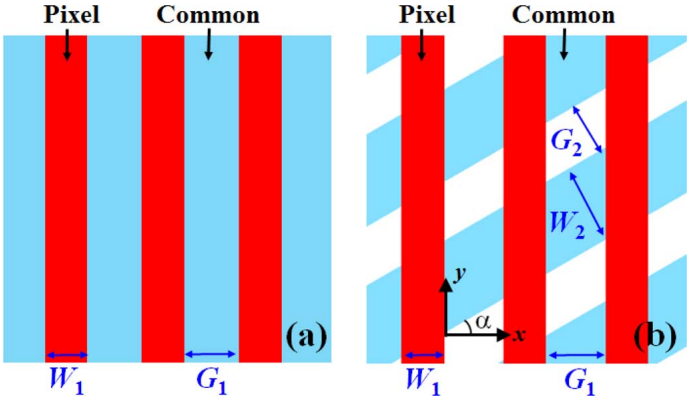

Figure 3.11: Schematic of PCFFS device structure [16]. ©2015, IEEE.

The switch ON mechanism of the new proposed cell was similar to the switch ON mechanism of the conventional FFS cell. However, the switch OFF procedure was differ-

ent. The voltage was withdrawn from the common electrodes and the pixel electrodes were kept floating, which simply refers to the fact that the voltages on the pixel electrodes are not kept fixed. A restoring pulse was applied in the opposite direction and this accelerated restoration of the LC moleculesn. The director deformation simulations were carried out by a commercial software and the 2×2 extended Jones matrix method was used to model the optics. Simulation results indicated that both the PCFFS and the FFS configurations had similar trends for the (voltage vs. transmittance) V-T curves. However, the director deformation was markedly different from the normal FFS configuration. The PCFFS configuration showed a multi domain distribution of directors in contrast to the conventional FFS that showed a 2-dimensional distribution. The conventional FFS cell had a wide viewing cone as a part of its inherent characteristics. The simulation results showed that both the conventional FFS cell and the PCFFS cell had the same wide viewing angles. The new configuration also showed a lot of fabrication tolerance as the V-T curves were found to be invariant with the physical dimensions and configuration of the common electrodes. As mentioned earlier, the PCFFS cells had a very short response time as compared to the conventional FFS cells.

In [17], Lien *et al.* pointed out that the conventional IPS panel might lead to a lowering of the display resolution as the display size was increased. They proposed a new device configuration combining a ridge fringe field effect and a multi-domain Vertical Alignment structure to create a high resolution full size display.

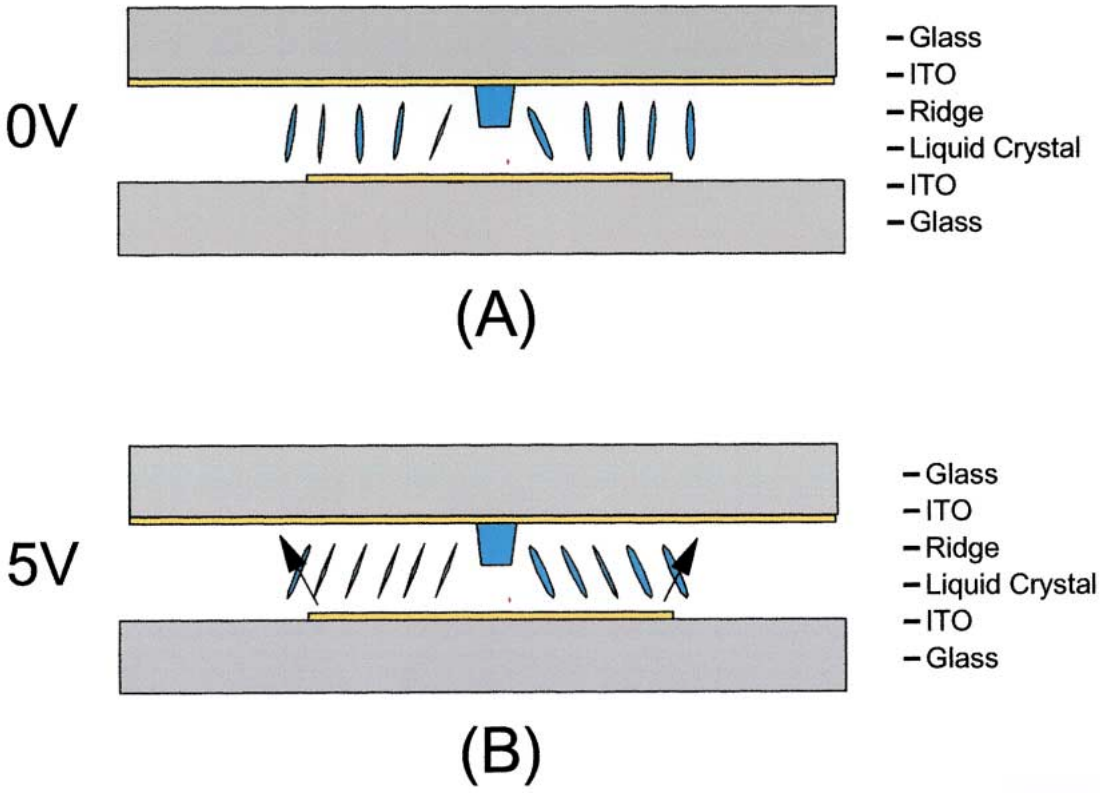

Figure 3.12: Schematic of ridge fringe field and multi-domain Vertical Alignment device structure [17].

Simulation based studies showed that the new device showed reasonably good picture fidelity and high resolution even at oblique viewing angles for large, full sized displays.

Chapter 4

Theory

4.1 Continuum Mechanics of Nematic Liquid Crystals

A nematic LC domain held undisturbed (no electrical or magnetic forces) at a particular temperature can be considered to be a closed system from the point of view of thermodynamics and can be considered to lie in a state of global thermodynamic equilibrium. Applying an electric or a magnetic field causes a deformation of the LC phase due to the inherent anisotropy of the liquid crystalline molecules. This makes the system depart from mechanical equilibrium causing restoring torques to act inside the domain. The free energy of the phase at this point can be assumed to be a function of a variable that characterizes the state of deformation of the system and the spatial gradients of this variable. The system can be considered to be back in equilibrium when this free energy has been minimised. Barbero and Evangelista gave a very detailed introduction to the continuum modelling of an LC domain [49].

It may be noted that an important disadvantage of this approach would be the inherent inability to look at a system when the departure from thermodynamic equilibrium is caused not solely due to a departure from mechanical equilibrium. For instance, at or near phase transitions or in the situation wherein isothermal conditions do not prevail, the above theory would have to be extended to include the temperature dependence of the free energy. However, for the modelling of LCD devices, such aspects may be neglected and the departure of the LC domain from equilibrium might be assumed to be solely due to mechanical deformations of the domain.

Frank's director deformation theory [30] is based upon the idea that the free energy of the LC domain depends solely on mechanical deformations from the equilibrium positions.

As such, any possible deformation or combination thereof may be considered to be a superposition of three fundamental deformation modes: *splay*, *twist* and *bend*. The free energy density functional f is expressed as:

$$f = f_0 + \underbrace{\frac{1}{2}K_{11}(\nabla \cdot n)^2}_{\text{Splay}} + \underbrace{\frac{1}{2}K_{22}(n \cdot \nabla \times n)^2}_{\text{twist}} + \underbrace{\frac{1}{2}K_{33}(n \times \nabla \times n)^2}_{\text{bend}} \tag{4.1}$$

One of the advantages of this theory is that the three different modes of deformation to be considered independently and the threshold electric fields for each mode of deformation to be calculated. The theory based on vector algebra and vector calculus is also more amenable to mathematical manipulations and computer simulations. While not suited for analysing LC phase transformations and also looking at defects in LC domains (defects are in fact, discontinuities in the director (n) field), they are accurate enough for to describe nematic bulk LC domains and have been the theory of choice for LCD researchers.

For the present work, the Landau-de Gennes Q tensor theory [29] has been used to model the continuum phase of the nematic LC. For a uniaxial nematic LC, the Q tensor is:

$$\mathbf{Q} = S\left(\mathbf{nn} - \frac{1}{3}\mathbf{I}\right) \tag{4.2}$$

where, S is the scalar order parameter, $\mathbf{n}$ is the director and $\mathbf{I}$ is the identity tensor.

Let the free energy density of the LC phase be represented by f. (Note: For the nematic phase, the free energy density, f may be taken as the difference in free energies between the nematic and the isotropic phases. This eliminates the need for an arbitrary constant of integration when the free energy density is integrated over the domain). The free energy density is a scalar and thus, its value must be independent of coordinate transformations. Thus, f must be a functional of the invariants of the tensor Q. However, as the Q tensor is traceless, the first invariant sums to zero and the other two invariants $trace(Q^2)$ and $trace(Q^3)$ are used in the expansion.

$$f = \frac{1}{2}A(\mathbf{Q} : \mathbf{Q}) - \frac{1}{3}B(\mathbf{Q}.\mathbf{Q}) : \mathbf{Q} + \frac{1}{4}C(\mathbf{Q} : \mathbf{Q})^2 + \frac{1}{2}L_1(\nabla\mathbf{Q}\vdots(\nabla\mathbf{Q})^T) + \frac{1}{2}L_2((\nabla\mathbf{Q}) \cdot (\nabla \cdot \mathbf{Q})) + \frac{1}{2}L_3\mathbf{Q} : (\nabla\mathbf{Q} : (\nabla\mathbf{Q})^T) + ... \tag{4.3}$$

The final three terms represent the contribution of the elastic energy to the total free energy of the LC phase. The elastic energy may be expressed in terms of invariants of the spatial derivatives of Q.

Strictly speaking, all of the bulk coefficients are dependent on temperature, but in general, only the temperature dependence of the first co-efficient is considered and expressed as:

$$A = A_0(T - T_{NI}) \tag{4.4}$$

where T_{NI} is the temperature at which the nematic phase starts becoming more stable than the isotropic phase.

The coefficients of the elastic terms in the Q tensor theory, L_1, L_2 and L_3 are not generally accessible experimentally. However, they can be related to the splay, twist and bend elastic constants if the value of the scalar order parameter S is a constant [50], [51]:

$$L_1 = \frac{3K_{22} - K_{11} + K_{33}}{6S_0^2} \tag{4.5}$$

$$L_2 = \frac{K_{11} - K_{22}}{S_0^2} \tag{4.6}$$

$$L_3 = \frac{K_{33} - K_{11}}{2S_0^3} \tag{4.7}$$

In the present work, a simplifying assumption has been made and only L_1 has been considered to be non-zero. This corresponds to the case in Frank's theory where the three constants, K_{11}, K_{22} and K_{33} are equal to each other.

Reorientation dynamics of the LC phase in LCDs depend on the application of a particular electric field from the electrodes. Under the influence of an electric field, the departure from equilibrium causes an increase in the free energy of the domain. Thus, additional terms must be included in the free energy expansion to take into account the contribution of the electric field towards the overall free energy of the domain. Thus, the full equation for the free energy density becomes [51]:

$$\begin{aligned} f = {} & \frac{1}{2}A(\mathbf{Q} : \mathbf{Q}) - \frac{1}{3}B(\mathbf{Q}.\mathbf{Q}) : \mathbf{Q} + \frac{1}{4}C(\mathbf{Q} : \mathbf{Q})^2 + \frac{1}{2}L_1(\nabla\mathbf{Q}\vdots(\nabla\mathbf{Q})^T) + \\ & \frac{1}{2}L_2((\nabla\mathbf{Q}) \cdot (\nabla \cdot \mathbf{Q})) + \frac{1}{2}L_3\mathbf{Q} : (\nabla\mathbf{Q} : (\nabla\mathbf{Q})^T) - \frac{\varepsilon_0}{8\pi}\left[\frac{\varepsilon_{||} + 2\varepsilon_\perp}{3}\mathbf{I} + (\varepsilon_{||} - \varepsilon_\perp)\mathbf{Q}\right] : \mathbf{EE} \end{aligned} \tag{4.8}$$

The free energy density must be integrated over the volume of the LC domain to give

the total free energy [51]:

$$F = \iiint_V \frac{1}{2}A(\mathbf{Q}:\mathbf{Q}) - \frac{1}{3}B(\mathbf{Q}.\mathbf{Q}):\mathbf{Q} + \frac{1}{4}C(\mathbf{Q}:\mathbf{Q})^2 + \frac{1}{2}L_1(\nabla\mathbf{Q}\vdots(\nabla\mathbf{Q})^T) + \frac{1}{2}L_2((\nabla\mathbf{Q})\cdot(\nabla\cdot\mathbf{Q})) + \frac{1}{2}L_3\mathbf{Q}:(\nabla\mathbf{Q}:(\nabla\mathbf{Q})^T) - \frac{\varepsilon_0}{8\pi}\left[\frac{\varepsilon_{||}+2\varepsilon_\perp}{3}\mathbf{I} + (\varepsilon_{||}-\varepsilon_\perp)\mathbf{Q}\right]:\mathbf{E}\mathbf{E}dV \tag{4.9}$$

4.1.1 Surface Anchoring

Anchoring in LC domains are mainly classified based upon the orientation of the LC molecules with respect to the surface normal. If the molecules are aligned along the surface normal, then the alignment is called *homeotropic* [52]. On the other hand, the alignment is called *planar* or *homogeneous* if the molecules are aligned parallel to the substrate, i.e-orthogonal to the surface normal. The LC domain in most LCD configurations has a *planar* surface alignment.

A commonly used method for aligning the LC molecules at the interface is by simple rubbing. The alignment direction of the molecules in the absence of external forces is referred to as the *easy axis*. Deviation of the molecules from the easy axis would cause a departure from equilibrium and cause an associated increase in the free energy. As the departure is solely due to mechanical forces, the free energy can be expressed in terms of the physical deformation. In order to make the surface energy expression compatible with the bulk free energy using the LdG theory, the following form may be used for the surface free energy [53]:

$$\gamma = \alpha_1(\mathbf{Q}:\mathbf{kk}) + \alpha_2(\mathbf{Q}:\mathbf{kk})^2 + ... + \beta_1(\mathbf{Q}.\mathbf{Q}):\mathbf{kk} + \beta_2((\mathbf{Q}.\mathbf{Q}).\mathbf{Q}):\mathbf{kk} + ... \tag{4.10}$$

For convenience , the series is truncated after the first term and the following form is used for simulations:

$$\gamma = \alpha(\mathbf{Q}:\mathbf{kk}) \tag{4.11}$$

The vector k in this case represents the *easy* axis, or, in other words, the direction along which the LC molecules would align in the absence of any electrical or magnetic fields. Similar to the bulk free energy density that is integrated over the entire volume to yield the total free energy, the surface energy density must be integrated over the entire boundary surface in order to obtain the total surface energy.

The anchoring of the LC molecules at the solid LC-boundary may be considered to be either of two types: *strong* or *weak* anchoring. For strong anchoring, anchoring strength at the interface is considered to be infinite and the surface alignment is considered to be invariant over the domain. Weak anchoring corresponds to a finite anchoring strength that may be overcome by electrical and other forces. Mathematically, strong anchoring corresponds to a Dirichlet boundary condition at the LC-solid interface. Use of the weak anchoring assumption with all the three elastic constants, L_1, L_2 and L_3 yields a set of differential algebraic equations (DAEs) that must be solved at the boundaries. Using the one constant approximation, ($L_2 = 0$ and $L_3 = 0$) simplifications lead to a Neumann boundary condition at the boundary.

4.1.2 Free Energy Minimiser

The equilibrium configuration of the LC phase is given by a Q tensor field that results in the free energy being minimised. Since, the free energy functional must be minimised and the principles of variational calculus can be used in order to minimise the free energy functional. The full procedure is given in [51], but the final equation has the form of the Euler-Lagrange equation as:

$$\frac{\partial f}{\partial Q} - \nabla . \left(\frac{\partial f}{\partial (\nabla Q)} \right) = 0 \tag{4.12}$$

Minimisation of the surface energy results in the boundary conditions of the problem given by:

$$\frac{\partial \gamma}{\partial Q} + \frac{\partial f}{\partial (\nabla Q)} . \mathbf{n} = 0 \tag{4.13}$$

In order to track the evolution of the domain with time starting from the initial conditions, a dynamic equation is needed in place of 4.12 that just gives the equilibrium configuration of the domain. The LHS of 4.12 is the first variation of the free energy functional (f) analogous to the first spatial derivative of physical quantities such as the momentum, energy and chemical potential in the more familiar transport equations of fluid mechanics, heat transfer and mass transfer, respectively [51] [49]. Furthermore, by a similar analogy, the LHS of 4.12 may be related to the time derivative of the free energy functional, f which in turn might be related to the time derivative of the $\mathbf{Q}$ as f is a functional of $\mathbf{Q}$. Dimensional analysis of both sides indicates that a quantity having the dimensions of viscosity must be multiplied to $\frac{\partial \mathbf{Q}}{\partial t}$. In the absence of flow, the only such quantity that comes into

play is the rotational viscosity μ. Thus, the final transient equation is given by:

$$-\mu\frac{\partial Q}{\partial t} = \underbrace{\frac{\partial f}{\partial Q} - \nabla.\left(\frac{\partial f}{\partial(\nabla Q)}\right)}_{\mathrm{M}} \tag{4.14}$$

In order to make the RHS compatible with the LHS, the quantities on the RHS must be traceless as $\frac{\partial Q}{\partial t}$ is a traceless tensor. Thus, in order to make the RHS traceless, the following modification must be made:

$$-\mu\frac{\partial Q_{ij}}{\partial t} = M_{ij} - \frac{1}{3}\cdot Trace(M_{ij}) \tag{4.15}$$

The equation is non-dimensionalised by making the following modification:

$$\tilde{T} = \frac{T}{T_{NI}}, \quad X = \frac{x}{l}, \quad \tilde{t} = \frac{t}{\tau}, \quad \tau = \frac{\mu}{a_0 T_{NI}}$$

4.2 Electric Field of Interdigitated Electrodes

The typical IPS LCD panel consists of interdigitated electrodes on only one side of the display panel. This results in an electric field that varies sinusoidally in space along the in-plane coordinate (parallel to the substrate) and decays exponentially in the through-plane (vertical) direction.

On account of the non-homogeneous nature of the electric field, a minimum of two dimensions is needed to model the IPS display pixel with sufficient accuracy. Given the actual dimensions of the LCD pixel, the interdigitated electrodes may be considered to be infinitely long and flat strips and edge effects such as fringing fields may be neglected. Furthermore, if the cross-talk between pixels is also neglected, then the entire structure can be simplified to a regular and repeating array of alternately charged electrodes. Simulation of this domain would involve considering a section with periodic boundary conditions at the two ends of the domain.

Past approaches have consisted of solving the Laplace equation given by Gauss law for a pre-determined director field configuration. This electric field is then used to calculate a new director field. The process is iterated until convergence is reached. But, this approach is very computationally intensive as it requires many iterations for convergence to be achieved.

For the present work, we use semi-analytical expressions developed in [54] to determine the electric field over the LCD domain. The Landau-de Gennes formulation that has been used in the present work reduces to a form wherein the change in the $\mathbf{Q}$ tensor domain with time is independent of the coupling between the electric field and the $\mathbf{Q}$ tensor field in the domain. Computationally this is advantageous as this reduces the number of back and forth iterations involving Gauss' law for the electric field and the expression for minimisation of the free energy in the LC domain. The following is the final equation derived for the spatial distribution of the voltage given by a set of interdigitated electrodes:

$$V(x,z) = \frac{4V_0}{\pi}\sum_{n=1}^{\infty}\frac{1}{2n-1}J_0\left(\frac{(2n-1)\pi s}{2a}\right)\cos\left(\frac{(2n-1)\pi x}{a}\right)\exp\left(-\frac{(2n-1)\pi|z|}{a}\right) \tag{4.16}$$

where, x is the in field (horizontal) coordinate, z is the through plane (vertical) coordinate, s is the spacing between electrodes, a is the sum of the electrode width and the spacing between electrodes and V_0 is the voltage applied between electrodes. $V(x,z)$ is the value of the voltage at coordinates (x,z). The electric field in the domain can be determined as the spatial derivative of the voltage field, such as:

$$E_x = -\frac{\partial V}{\partial x} \tag{4.17}$$

$$E_z = -\frac{\partial V}{\partial z} \tag{4.18}$$

which gives,

$$E_x = \frac{4V_0}{\pi}\sum_{n=1}^{\infty}\frac{1}{2n-1}J_0\left(\frac{(2n-1)\pi s}{2a}\right)\sin\left(\frac{(2n-1)\pi x}{a}\right)\frac{(2n-1)\pi}{a}\exp\left(-\frac{(2n-1)\pi|z|}{a}\right) \tag{4.19}$$

and,

$$E_z = \frac{4V_0}{\pi}\sum_{n=1}^{\infty}\frac{1}{2n-1}J_0\left(\frac{(2n-1)\pi s}{2a}\right)\cos\left(\frac{(2n-1)\pi x}{a}\right)\frac{(2n-1)\pi}{a}\exp\left(-\frac{(2n-1)\pi|z|}{a}\right) \tag{4.20}$$

The electric field, as seen in the figure 4.1 shows a periodic variation along x and an exponential decay along z as expected.

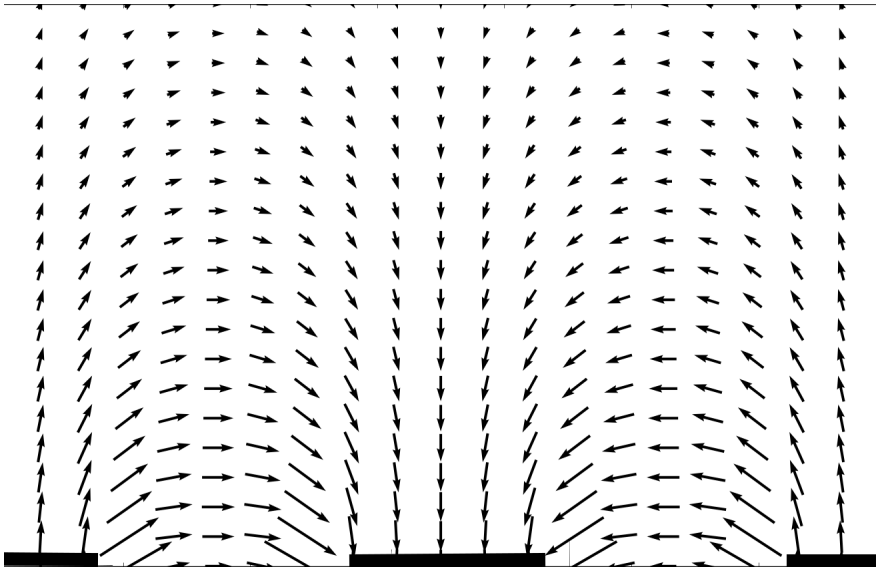

Figure 4.1: Electric field produced by a set of interdigitated electrodes of width 3 μ and spacing 4μ. Voltage of 5.0V is applied between electrodes. A snapshot of the domain is shown. The field in the regions directly above electrodes is vertical direction while the field in the inter-electrode region is in the horizontal direction.

The electric field in regions directly above the electrodes points vertically upward or downward whilst the electric field in between electrodes lies in a direction parallel to the domain.

Chapter 5

Dynamic Studies and Comparison Between Strong and Weak Anchoring

5.1 Definition of Tilt and Twist Metrics

The transmissivity of the LCD pixel depends on the orientation of the LC domain. The presence of the two crossed polarisers at the two ends of the domains ensure that only light polarised along a certain axis would pass through the pixel to reach the user. The twist of the LC domain, in the wave-guiding regime, ensures that light gets polarised along the proper coordinate and is allowed to pass through the second polariser. For the light to undergo wave-guiding, it must encounter birefringence in the domain. The two indices of refraction in a birefringent medium are given by [27]:

$$n = n_0 \tag{5.1}$$

for the O wave (polarised perpendicular to the optic axis) and,

$$\frac{1}{n^2} = \frac{\cos^2\theta}{n_0^2} + \frac{\sin^2\theta}{n_e^2} \tag{5.2}$$

for the E wave (polarised parallel to the optic axis).

θ is the angle formed by the direction of light and the optic axis. For a vertically inclined (tilted) domain, θ is 0 and hence, both the refractive indices become equal. This removes birefringence from the LC domain. The light passes through the domain as it would pass through any isotropic material and does not undergo wave-guiding. Thus the

polarisation vector of the light does not undergo any change in orientation as light propagates through the domain and the light gets blocked off by the second, crossed polariser (crossed with respect to the first polariser). The transmissivity of the domain is indicated by the amount of "twist" (horizontal alignment) in the domain. For an IPS configuration, the domain alternates between regions of vertical and horizontal alignment. Regions having predominantly horizontal alignment are expected to have a higher transmissivity.

In the absence of an optics code that would allow us to calculate the transmissivity at different points in the IPS pixel, metrics were developed to indicate how close the simulated IPS domain was to an equivalent domain that is oriented horizontally. Let $n(x, y, z)$ be the director field.The ideally oriented domain has a director configuration that can be represented as:

$$\mathbf{n_i} = 1\mathbf{e_x} + 0\mathbf{e_y} + 0\mathbf{e_z} \tag{5.3}$$

where z is the through plane coordinate and x is the horizontal coordinate. The simulated director configuration of the IPS domain would show a highly non-homogeneous orientation. However, alternate regions having predominantly horizontal or vertical alignment also exist. Let the simulated domain be represented by:

$$\mathbf{n_s} = n_x\mathbf{e_x} + n_y\mathbf{e_y} + n_z\mathbf{e_z} \tag{5.4}$$

where n_s is the simulated LC domain in the IPS pixel and n_x, n_y and n_z are the components of the director field along the three coordinates. The "twist" metric, η_{twist} that quantifies how close the simulated domain is close to a completely horizontally oriented domain can then be defined as:

$$\eta_{twist} = \frac{\int_0^d n_i \cdot n_s dz}{\int_0^d dz} \tag{5.5}$$

For a discrete domain, the above reduces to:

$$\eta_{twist} = \frac{\sum_1^N \mathbf{n_i} \cdot \mathbf{n_s}}{N} \tag{5.6}$$

where N is the total number of grid points in the vertical direction.

For a uniformly twisted horizontal domain, the value of η_{twist} would come out to be 1, while that for a domain completely tilted vertically,the metric would come out to be 0.

Another metric is defined in a manner similar to η_{twist} that quantifies how close the simulated domain is to a completely vertically tilted domain. Such a domain may be represented as:

$$\mathbf{n_i} = 0\mathbf{e_x} + 0\mathbf{e_y} + 1\mathbf{e_z} \tag{5.7}$$

As before, the simulated IPS domain configuration is given by $\mathbf{n_s}$. Thus, the "tilt" metric may be defined as:

$$\eta_{tilt} = \frac{\int_0^d n_i \cdot n_s dz}{\int_0^d dz} = \tag{5.8}$$

again, for a discrete domain, this reduces to:

$$\eta_{tilt} = \frac{\sum_1^N \mathbf{n_i} \cdot \mathbf{n_s}}{N} \tag{5.9}$$

where N is the number of points in the vertical direction.

As explained earlier, the regions having a high value of η_{tilt} would have a very low transmissivity as the light passing through these portions of the domain would not experience birefringence. The LC domain in the OFF state has uniform alignment. As voltage is applied between the electrodes, the horizontal and vertical components of the electric field cause the LC domain to alternately *twist* and *tilt*. The dynamics of the re-alignment need to be studied as it has a direct bearing to the response time of the pixel. Ideally, a pixel should have as low a response time as possible to prevent latency. If the response time is too large, then it might lead to a lag and ghosting of images.

Studies have also been carried out to analyse the effect of the surface anchoring on the LC domain (if any). As pointed out earlier, strong and weak anchoring are the two main types of anchoring at the LC-substrate interface. Simulations were carried out with both Dirichlet and Neumann boundary conditions to look at the dynamic characteristics of the domain.

Thus, to summarise, the broad objectives of this chapter are as follows:

1. Comparison between strong and weak anchoring
2. Dynamic study of pixel deformation

5.2 Comparison Between Strong and Weak Anchoring

The simulation of the LC domain is done with the python package GSML developed in house [55]. This package implements a spectral collocation solver that transforms the PDEs to a set of ODEs that are then solved by a solver called vode available in the python

package scipy. The ODE solver uses an implicit Adams method for non-stiff problems and backward differentiation formula for stiff problems. The Euler-Lagrange equation and the equations for the weak anchoring boundary conditions are solved using this numerical method.

Thermodynamic and elastic constants for the liquid crystalline material E7 have been used for the simulations. The values of the thermodynamic constants A,B and C based upon those in literature have been used [56]. Isothermal conditions have been assumed to prevail in the domain at a temperature of 306K. The elastic constants L_2 and L_3 become equal to zero due to the assumption that all the Frank's elastic constants are equal. At the boundaries, both strong and weak anchoring were evaluated. Strong anchoring was enforced by setting $\frac{\partial \mathbf{Q}}{\partial t}$ to zero at the boundaries. This ensures that the $\mathbf{Q}$ tensor at points adjacent to the boundary does not change with time. Weak anchoring was evaluated with an anchoring strength of 1×10^{-6}.

A Q tensor field is created for every point in the LC domain. The software package Paraview[57] has been used to visualise the Q tensor domain using tensor glyphs. The glyphs represent a rank-2 tensor by means of its eigenvalues and eigenvectors. For uniaxial nematics, the largest eigenvalue gives the scalar order parameter, S and this value is used to scale the glyph. The corresponding eigenvector gives the director configuration, n at that point and this determines the orientation of the glyph at that point.

The strong anchoring assumption physically implies that the alignment of the LC domain at the LC-substrate interface is completely fixed. In other words, the anchoring strength between the LC molecules and the glass substrate is considered to be infinite. Mathematically, this translates to Dirichlet boundary conditions where the $\mathbf{Q}$ tensors of the molecules at the boundaries are fixed.

Weak anchoring implies the anchoring strength between the LC molecules and the glass substrate is finite. The surface anchoring energy needs to be minimised using principles of variational calculus and which leads to a Neumann boundary condition of the LC domain at the interface.

The free energy at the interface depends on the bulk Euler-Lagrange equation as well as the boundary conditions. For larger values of the anchoring strength coefficient at the boundary, the orientation of the $\mathbf{Q}$ tensor at the domain is drastically different from the orientation of the $\mathbf{Q}$ in the adjacent layer. This closely resembles the strong anchoring assumption at the boundaries.

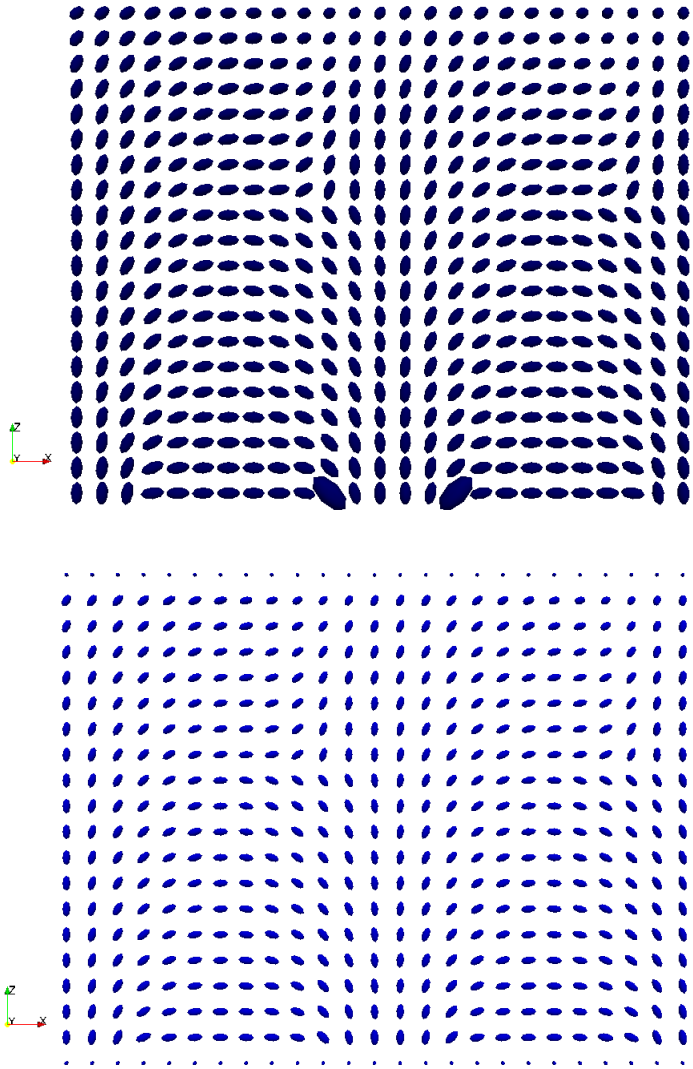

Figure 5.1: The two figures show the schematics of an IPS LC domain for weak (top) and strong anchoring (bottom) respectively. The voltage applied is 5V, electrode spacing is 2μ and depth of pixel is 3μ.

5.3 Dynamic Response of the LC Domain

The dynamics of the LC domain significantly affect the response time of the LCD pixel. For ideal operations, response times must be as low as possible. A higher response time would result in effects such as halos and ghosting on the screen. It may be pointed out at this point that the response time is considered to be one of the inherent weaknesses of the IPS pixel configurations, especially in high performance conditions such as gaming and fast moving television displays.

The simulations were carried out at an approximate temperature of $306K$ that is just below the nematic-isotropic transition point for E7. Material properties for E7 was used in the simulations. To carry out the dynamic simulations, the domain was visualised at dimensionless times $\tau = 5000$ to $\tau = 90000$. The metrics were also extracted for the domain at these values and the evolution of the metrics in time was examined to gain an idea of the response time of the domain. The results of the visualisations and the metric plots have been summarised in the following paragraphs.

From the schematics, it can be seen that the switching behaviour of the liquid crystalline domain is directly affected by the applied electric field. As the electrodes are present at only one side of the domain, the electric field decreases exponentially in magnitude as one moves away from the electrode in the vertical direction. Thus, the LC molecules in the domain closer towards the electrodes experience much stronger electric field and thus, switching of the domain takes place much faster close to the electrode. Regions of the domain further away switch much more slowly on account of the fact that the electric field is much weaker there and more time is taken for the electric field to overcome the inertial forces in the LC domain.

LCDs generally use *p-type* liquid crystals. In other words, $(\varepsilon_{||} - \varepsilon_{\perp})$ is positive for these LCs. Thus, upon actuation by an electric field, these LCs orient in the direction of the field. For the fully switched LC domain, the orientation of the molecules mimic the electric field in the domain.

As the IPS LCD domain shows alternate regions of horizontal(in-plane) twist and vertical(through plane) tilt, it is expected that the twist and the tile metrics show a periodic and alternate pattern of variation (alternate crests and troughs) across the domain. For larger domains(greater pixel depth) and lower electric field magnitudes, the twist or the tilt is expected to be shallower.

The regions of higher twist correspond to a higher transmissivity of the LCD pixel while conversely, the regions having a higher vertical tilt correspond to lower values of

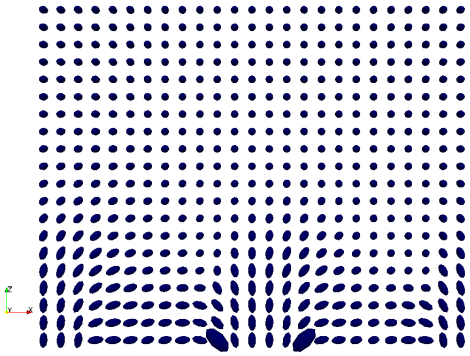

Figure 5.2: (a) t=1.2ms

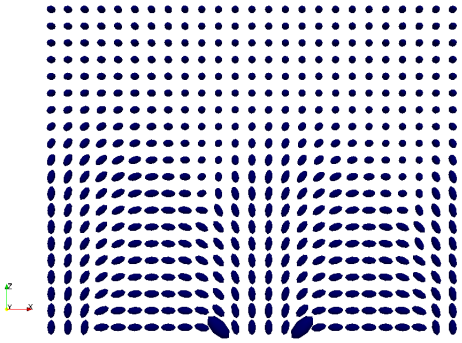

Figure 5.3: (b) t=3.6ms

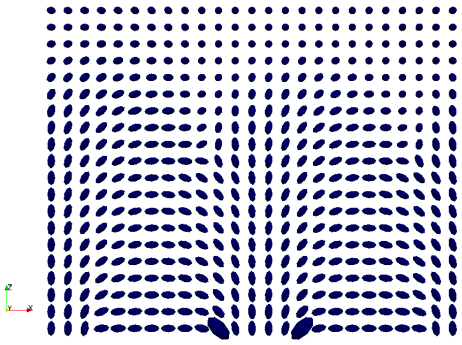

Figure 5.4: (c) t=8.4ms

Figure 5.5: Schematic of domain at three different times, 1.2 ms, 3.6 ms and 8.4 ms (starting from the top) showing the evolution of domain deformation with time. The voltage applied is 5V, electrode spacing is 2μ and depth of pixel is 3μ

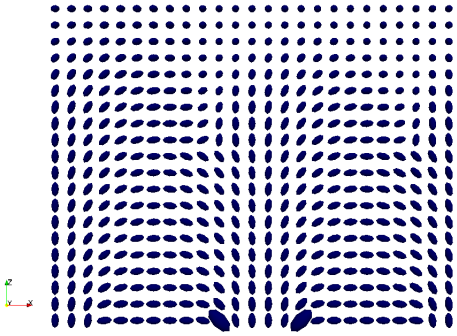

Figure 5.6: (d) t=10.8 ms

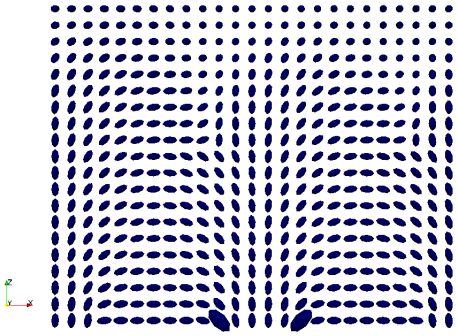

Figure 5.7: (e) t=12 ms

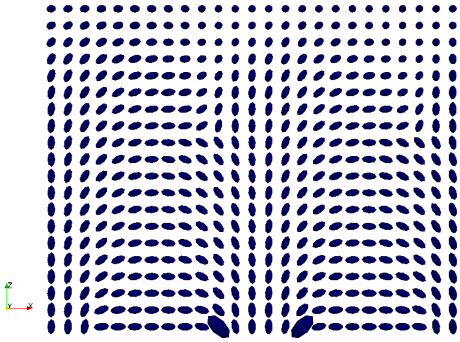

Figure 5.8: (f) t=14.4 ms

Figure 5.9: Schematic of domain at three different times, 10.8 ms, 12 ms and 14.4 ms (starting from the top) showing the evolution of domain deformation with time. The voltage applied is 5V, electrode spacing is 2μ and depth of pixel is 3μ

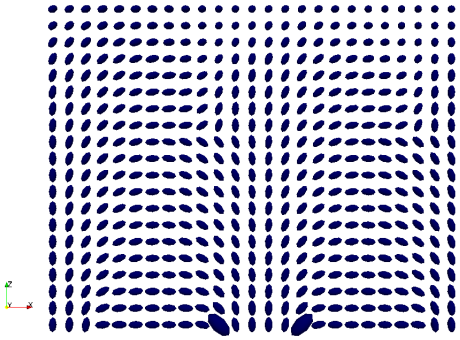

Figure 5.10: (g) t = 16.8 ms

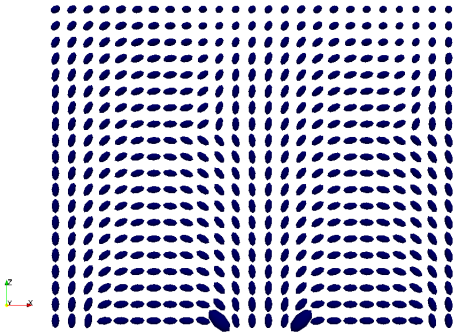

Figure 5.11: (h) t = 19.2 ms

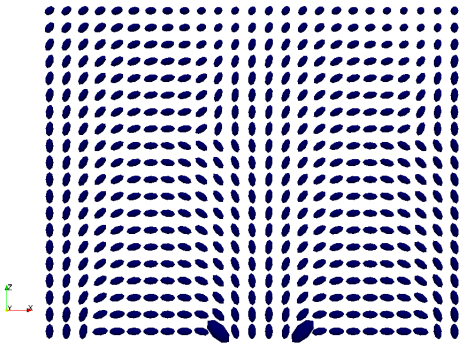

Figure 5.12: (i) t = 21.6 ms

Figure 5.13: Schematic of domain at three different times, 16.8 ms, 19.2 ms and 21.6 ms (starting from the top) showing the evolution of domain deformation with time. The voltage applied is 5V, electrode spacing is 2μ and depth of pixel is 3μ

transmissivity. So, it is desirable for the pixel to have a wider regions of twist as this would imply a higher overall transmissivity over the entire domain.

The IPS LCD domain shows very little region where the domain is predominantly twisted. Thus, it might be concluded that in order to have better performance, one needs to have wider spacings between electrodes as these regions between electrodes promote in plane twisting while regions directly above electrodes promote vertical alignment. In conclusion, the electrode spacing should be larger than the electrode width.

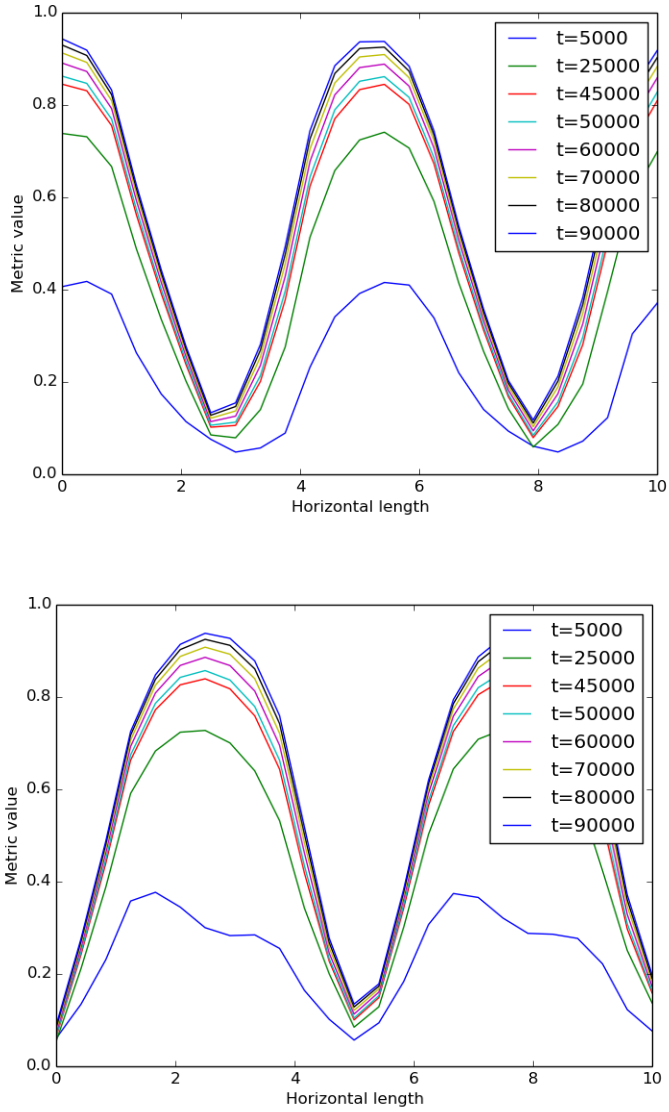

Figure 5.14: The evolution of the tilt (top) and tilt (bottom) metrics over time for the LC domain. It can be seen that the response is non linear and the deformation slowly attains equilibrium over time.

Chapter 6

Parametric Study of the Equilibrium Configuration of the IPS Domain

The equilibrium orientation of the LC domain is governed by its intrinsic geometry and the electric field applied to the domain. Apart from the voltage strength applied between the electrodes, the electric field also depends on the electrode width, electrode spacing and depth of the LC domain.

In this section, we investigate the effects of the parameters below on the equilibrium orientation of the LC domain. The three metrics used in the previous chapter are used to quantify the equilibrium orientation.

- Effect of applied voltage.
- Effect of electrode spacing.
- Effect of pixel size on domain
- Effect of electrode width

6.1 Effect of Applied Voltage

The reorientation of the domain proceeds upon actuation by the electric field. The process of reorientation is actually the end result of the competing forces of the electric field and the restoring forces arising due to the elasticity of the domain.

Thus, the electric field aims to re-orient the domain along its direction whilst the elastic forces oppose this motion. A threshold field exists beyond which the electric field overcomes the restoring forces. The IPS LC domain mainly undergoes the *twist* and the *bend* types of mechanical deformations. Accurate calculations of the threshold voltages would involve moving away from the one-constant approximation that has been made in the present work. In other words, we should remove the assumption that the *splay*, *twist* and *bend* elastic constants are equal. The L_2 and L_3 constants in the full LdG expansion would become non-zero and the boundary conditions would evolve to a set of differential algebraic equations (DAEs) to be solved at every point in the domain boundaries.

Simulations were run at 1,2.5 and 5 V applied between the electrodes. In general, voltages near the upper limit of 5V are used to drive LCD pixels. The choice of these three voltages was made to select a very low voltage (below threshold voltage), an intermediate voltage and the normal operating voltage. The deformation of the domain was compared at the three voltages. The results showed an expected trend as the higher voltages lead to greater twist and tilt. Also, at higher voltages, the twist penetrated deeper into the domain. This is due to the fact that the electric field decreases exponentially in magnitude as we move up the domain. At higher voltages, the voltage deeper into the domain is still above the threshold and thus, the twist penetrates deeper.

The metrics defined earlier have been used to quantify the effect of the applied voltage on the pixel domain. The following figures give the equilibrium metrics pattern at voltages of 1, 2.5 and 5V applied between electrodes. The electrode spacing is 2μ and the pixel depth is 3μ.

As expected, the twist and the tilt metrics both show larger values at higher voltages. Physically, this corresponds to greater deformation of the LC domain upon application of a larger electric field.

The metrics also indicate that the deformation of the domain does not bear a linear relationship with the applied voltage. The non-linear relationship is to be expected beyond the threshold voltage as the deformation of the domain is due to a complex interplay of various forces and the electric field.

It should also be pointed out that the concept of a threshold voltage is not very useful for the IPS configuration. A more useful quantity is a threshold electric field since the effective electric field would change for IPS with changes in the physical dimensions of the pixel domain even for constant values of the voltage.

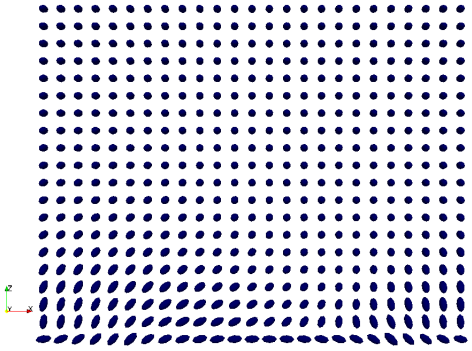

Figure 6.1: The schematic for an IPS LC domain for voltage=1V

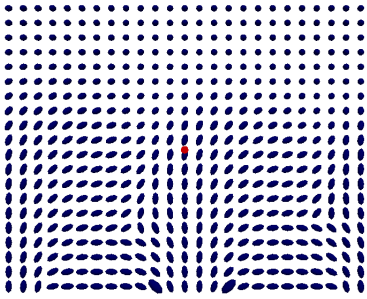

Figure 6.2: Schematic for IPS LC domain for voltage=2.5V

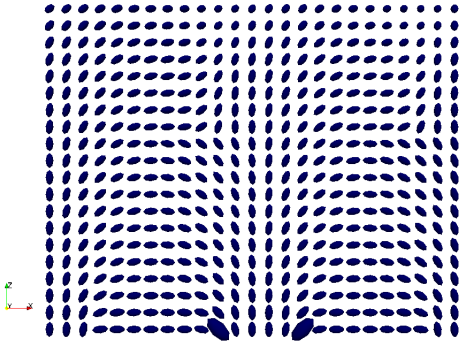

Figure 6.3: Schematic for IPS LC domain for voltage=5V

Figure 6.4: Schematic of domain at three different applied voltages, 1V, 2.5V and 5V (starting from the top) electrode spacing is 2μ and depth of pixel is 3μ for all the three cases. The schematics clearly show that as the voltage increases, the deformation penetrates further into the domain. This is according to the expected trends

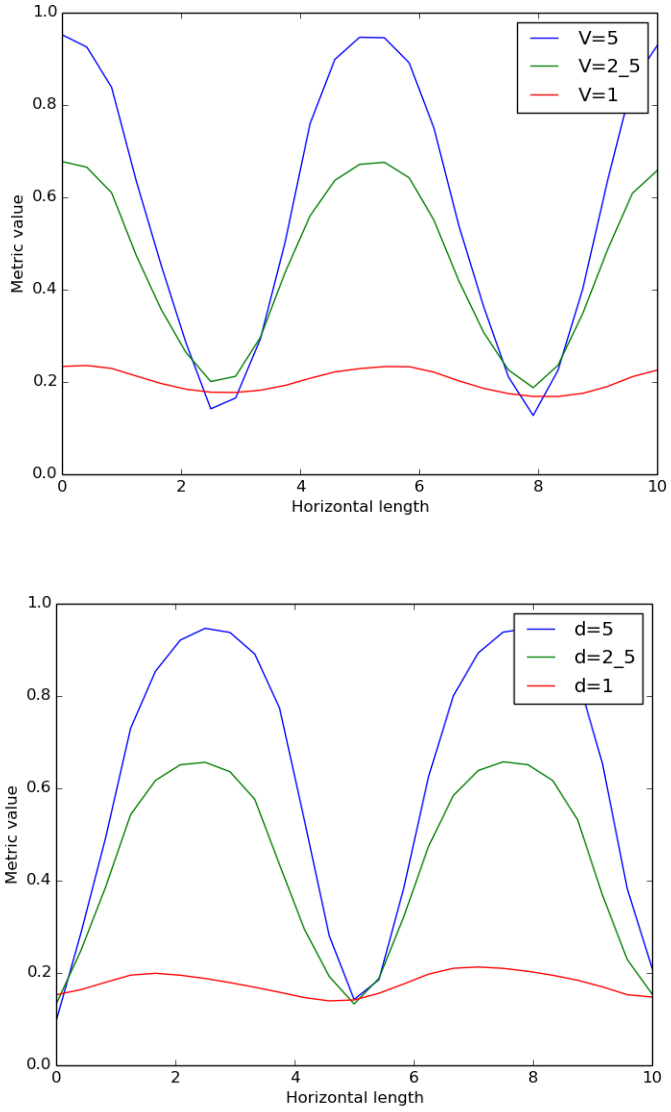

Figure 6.5: The evolution of the tilt (top) and the twist (bottom) metrics in the domain for three different voltages. Other parameters such as the electrode spacing and the pixel depth are kept constant. Metrics show that the deformations, both twist and tilt penetrate deeper into the domain as the voltage increases.

6.2 Effect of Pixel Depth

As the characteristic electric field produced by the interdigitated electrodes decays exponentially down the domain, the effect of the pixel depth on the equilibrium orientation of the domain is obvious. As smaller domain would have most of the LC material deformed, whereas a larger domain would leave some portion of the domain (the portion on the viewer side) non-deformed.

Simulations were carried out for three values of the pixel depth: $3\mu, 4\mu$ and 5μ. As expected, the domain at 3μ exhibits the most deformation while the domain at 5μ shows the least deformation.

The choice of the three values of pixel depth are governed by constraints involving the pixel deformation and the ease of manufacturing of the pixels. A smaller pixel depth is more desirable in terms of the deformation, i.e- the smaller the pixel, the deeper is the penetration of the electric field into it. A highly deformed domain is preferable from a point of view of the performance of the pixel.

We use the same metrics as before to analyse the dependence of pixel deformation on the pixel depth. We present the results for applied voltage = 5V, electrode spacing = 2 μ. Three values of the pixel depth were analysed: 3,4 and 5 μ.

The electric field for a given voltage and electrode configuration would have a fixed penetration. Increasing the pixel depth beyond the field penetration just adds more LC that stays unswitched to the domain. Thus, manufacturing constraints permitting a smaller pixel is always preferable.

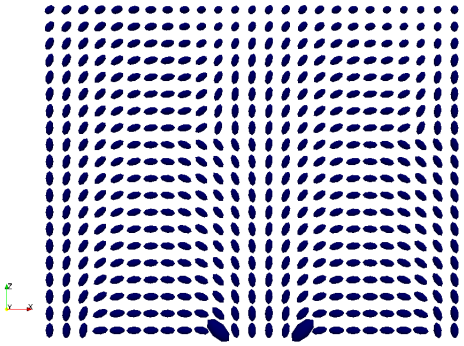

Figure 6.6: The schematic for an IPS LC domain for pixel depth=3μ

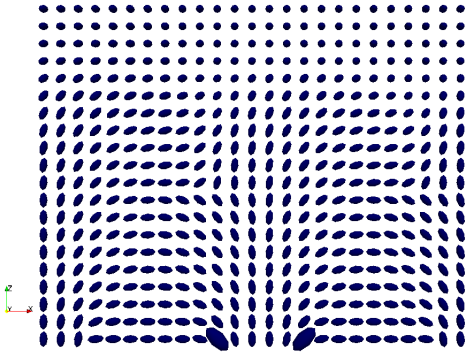

Figure 6.7: Schematic for IPS LC domain for pixel depth=4μ

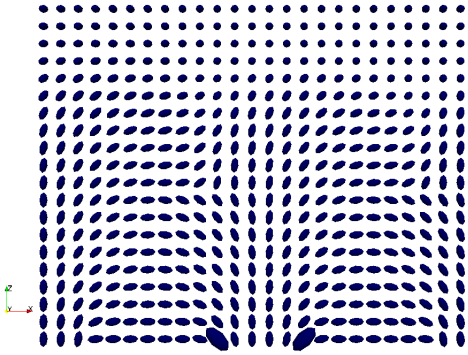

Figure 6.8: Schematic for IPS LC domain for pixel depth=5μ

Figure 6.9: Schematic of domain at three different pixel depth, 3μ, 4μ and 5μ (starting from top) electrode spacing is fixed 2μ and applied voltage at 5V. As the size of the pixel increases, more of the domain remains beyond the reach of the threshold voltage and thus does not undergo deformation.

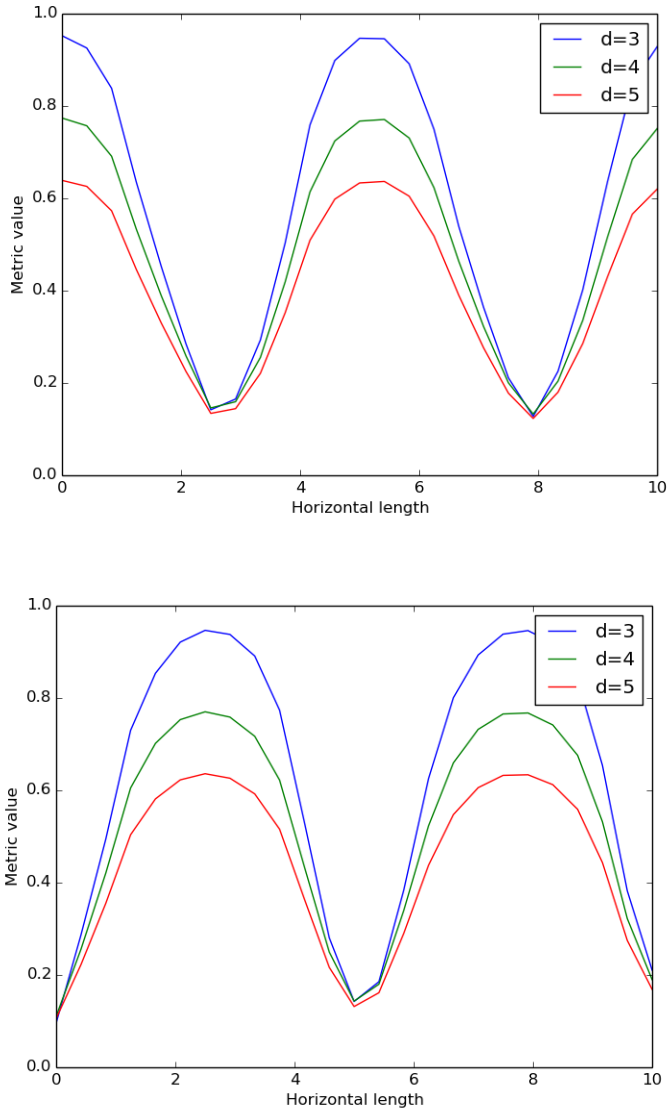

Figure 6.10: The evolution of tilt (top) and twist (bottom) metrics over three different pixel depths. Other parameters such as the applied voltage and the electrode spacing are fixed at 5V and 2μ.The metrics clearly show that for the larger domain, more of the domain remains undeformed.

6.3 Effect of Electrode Spacing

Spacing electrodes wide apart reduces the overall electric field strength in the pixel for a given value of the applied voltage and electrode configurations. However, as pointed out earlier, it is not just the electric field, but also the direction of the electric field that is important from the point of view of operation of the LCD pixel. For the IPS mode, it is more desirable to have a horizontal *twist* than a vertical reorientation *tilt*. Spacing the electrodes further apart does indeed force a greater volume of the domain to *twist* instead of *tilt*.

The following figures show the domain orientation for an applied voltage of 5V for three different electrode spacings: 2μ, 4μ and 6μ. The metric based analysis pattern for the three cases of electrode spacing is given in the following figures. It can be seen that as the electrode spacing increases, the tilt metric experiences a pronounced transformation. This is due to the combined effect of the net electric field decreasing in magnitude as the electrodes move farther apart and due to higher amount of horizontal field as the electrodes move further apart.

The results for this particular parametric analysis are a bit surprising. Looking at the metrics, it can be seen that changing the electrode spacing has only a very small effect on the domain. This might be due to the fact that with the electrodes spaced further apart, the strength of the electric field decreases and this negates any change in the *twist* of the domain.

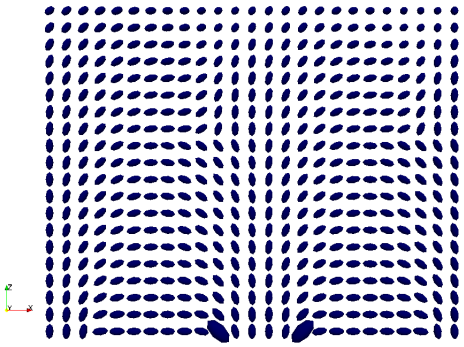

Figure 6.11: The schematic for an IPS LC domain for electrode spacing=2μ

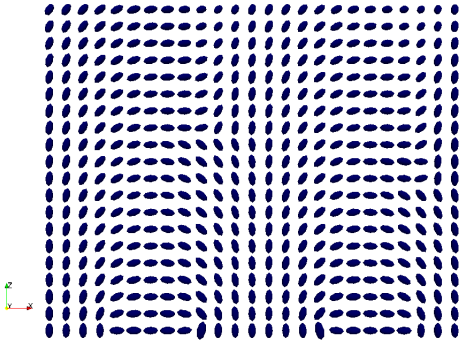

Figure 6.12: Schematic for IPS LC domain for electrode spacing=4μ

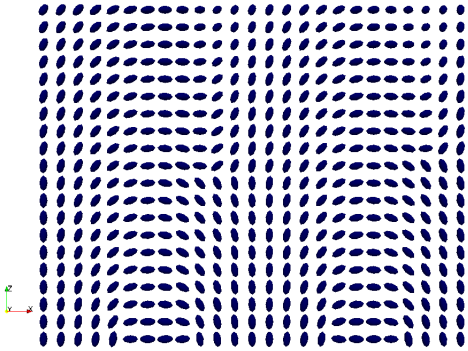

Figure 6.13: Schematic for IPS LC domain for electrode spacing=6μ

Figure 6.14: Schematic of domain at three different electrode spacings, 2μ, 4μ and 6μ (starting from the top), pixel depth is 3μ and applied voltage is 5V. The domain does not show any drastic change with the change in the three values for the electrode spacing.

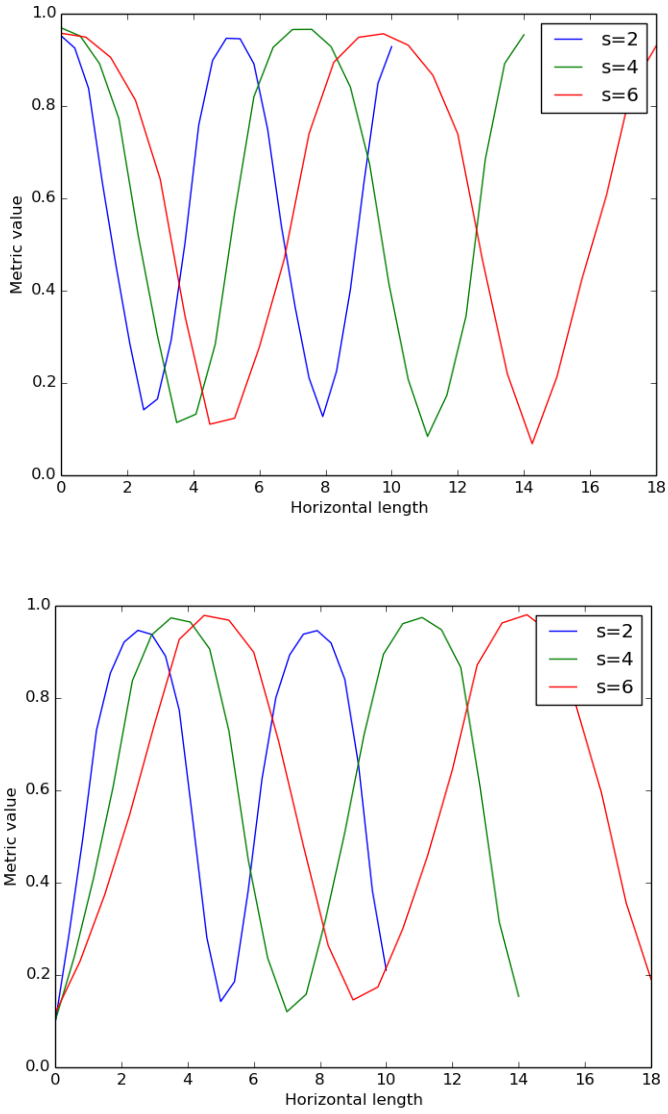

Figure 6.15: The tilt (top) and the twist (bottom) metrics for the three different electrode spacings, 2μ, 4μ and 6μ. The applied voltage and the pixel depths are kept constant. Simulations were carried out such that each simulation comprises of two half electrodes on the ends, a full electrode in the centre and the regions in between. The change in the electrode spacing causes a change in the overall size of the domain.

6.4 Effect of Electrode Width on the Domain

The effect of the electrode width on the domain was also studied. A wider electrode is expected to cause more deformation of the domain due to a higher average electric field. We looked at the deformation caused by three different values of electrode width, 2μ, 3μ and 4μ. Furthermore, having the electrode width much larger than the electrode spacing would cause the domain to *tilt* and this would in turn, negatively affect the LCD performance.

Metrics defined earlier were used to analyse the deformation of the domain at three different values of the electrode width. It is expected that both the twist and the tilt metrics would have the highest value for the 4μ case as the domain has the greatest deformation for this value of the electrode width. The metric values calculated confirm this trend.

The increase in the electrode width has an expected effect on the LC domain. Both the twist and the tilt metrics show that the domain deformation has penetrated deeper into the domain. Thus, the fact that an increase in the electrode width provides a greater area over which the deformation occurs in the domain. Also, the effective magnitude of the electric field in the domain increases.

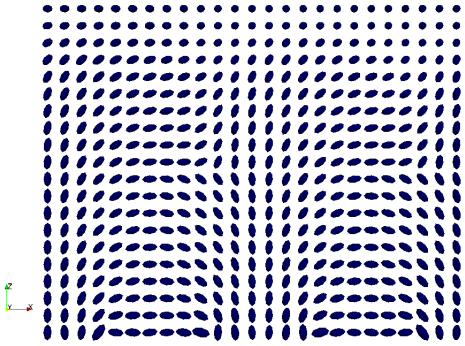

Figure 6.16: The schematic for an IPS LC domain for electrode width=2μ

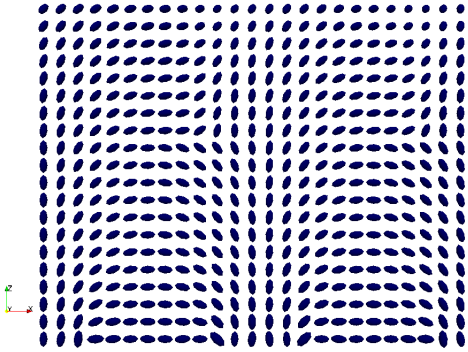

Figure 6.17: Schematic for IPS LC domain for electrode width=3μ

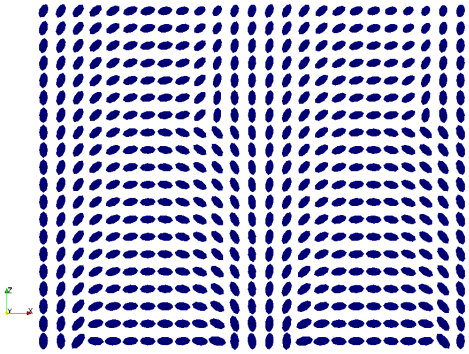

Figure 6.18: Schematic for IPS LC domain for electrode width=4μ

Figure 6.19: Schematic of domain at three different electrode widths,2μ, 3μ and 4μ, (starting from the top), pixel depth is 3μ, electrode spacing is 2μ and applied voltage between electrodes is 5V. Increasing the electrode width increases the overall electric field in the volumetric domain.

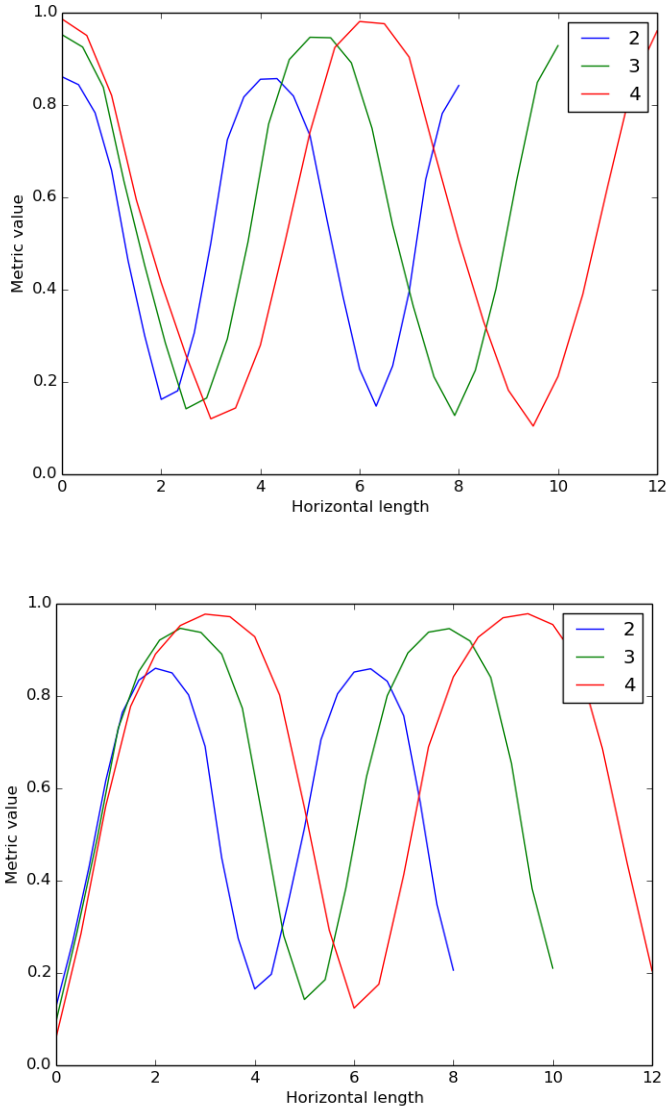

Figure 6.20: Tilt (top) and twist (bottom) metrics for the LC domain for three different electrode widths 2μ, 3μ and 4μ. the applied voltage, the electrode spacing and the pixel depth are kept constant as before. Also, as in the previous case, due to an increase in the electrode width, the overall size of the domain increases.

Chapter 7

Conclusions and Recommendations

7.1 Conclusions

In this work a nematic dynamics simulation method was developed and used to examine the effect of key design and operating parameters on IPS pixel performance. The deformation metrics showed the following trends:

- The deformation of the nematic domain increased for higher electrode voltages. Both the *twist* and *tilt* metrics increased with higher potential.
- Increasing the pixel depth has significant effect at depths below the penetration length scale of the maximum field. For pixel depths above this value, there is little effect on nematic regions above the depth and performance metrics decrease with increasing depth as a result.
- The increase in the electrode spacing had very little effect on the domain. This might be due to the fact that any increase in electrode spacing lowered the overall electric field and this compensated for any change in the *twist* or tilt metric.
- Changing the width of the electrodes increased the overall electric field in the domain. Furthermore, each individual electrode also influenced a greater region of the domain and this increased the deformation of the LC domain.

7.2 Recommendations

Recommendations for future work are focused on increasing the fidelity of the model used for nematic dynamics simulations. Some areas of further improvement include:

- *Boundary Conditions*- Although the less common and more complicated assumption of weak anchoring at the interfaces has been used in this work, the simplifying assumption involving the fact that all the elastic constants- K_{11}, K_{22} and K_{33} are equal had to be made keeping in mind time constraints. This allowed for the boundary equations to be expressed as conventional Neumann boundary conditions. More accurate simulations would involve removing the simplifying assumption. However, that would call for the solution of a series of differential algebraic equations(DAEs) at the interface. Since this is not currently supported in either scipy or GSML, other software packages may be used in addition to these two to simulate the domain.

- *Optics*-The optical performance and characteristics of the LCD domain can be directly correlated to the deformation of the LCD pixel. Matrix-based methods can be used to model the optical transmittance of the cell with a sufficient degree of accuracy. Full-scale simulations that involve solving Maxwell's equations numerically are not generally required for analyses of LCDs.

  The matrix methods such as extended Jones can be added on top of the present code to determine the optical transmittance. The optics code can also be developed independently as it would only require the final output of the present code as an input.

References

[1] Paul Semenza. Display marketplace: A new chapter for the display market,. *Information Display*, 26(5), 2010.

[2] Jaume Garcia-Amoros and Dolores Velasco. *Polysiloxane Side-Chain Azobenzene-Containing Liquid Single Crystal Elastomers for Photo-Active Artificial Muscle-Like Actuator in Advanced Elastomers - Technology, Properties and Applications*. INTECH-Open, 2012.

[3] Kebes. https://en.wikipedia.org/wiki/liquid_crystal#/media/file:liquidcrystal-mesogenorder-nematic.jpg.

[4] C. J. Barrett. http://barrett-group.mcgill.ca/tutorials/liquid_crystal/lc04.htm.

[5] M. W. Geis, P. J. Bos, V. Liberman, and M. Rothschild. Broadband optical switch based on liquid crystal dynamic scattering. *Optics Express*, 24(13):13812–13823, 2016.

[6] Ilias Pappas, Stylianos Siskos, and Charalambos A. Dimitriadis. *Active-Matrix Liquid Crystal Displays - Operation, Electronics and Analog Circuits Design in New Developments in Liquid Crystals*. InTech, 2009.

[7] Jin Seog Gwag, Kyunghwa Sohn, Young-Ki Kim, and Jae-Hoon Kim. Electro-optical characteristics of a chiral hybrid in-plane switching liquid crystal mode for high brightness. *Optics Express*, 16(16):12220–12226, 2008.

[8] Dave3457 - own work, public domain, https://commons.wikimedia.org/w/index.php?curid=9862713.

[9] Zhibing Ge, Shin-Tson Wu, Seong Su Kim, Ji Woong Park, and Seung Hee Lee. Thin cell fringe-field-switching liquid crystal display with a chiral dopant. *Applied Physics Letters*, 92:181109, 2008.

[10] Zhibing Ge, Thomas X. Wu, Ruibo Lu, Xinyu Zhu, Qi Hong, and Shin-Tson Wu. Comprehensive three-dimensional dynamic modeling of liquid crystal devices using finite element method. *IEEE Journal of Display Technology*, 1(2):194–, 2005.

[11] Ruibo Lu, Shin-Tson Wu, Zhibing Ge, Qi Hong, and Thomas X. Wu. Bending angle effects on the multi-domain in-plane-switching liquid crystal displays. *IEEE Journal of Display Technology*, 1(2), 2005.

[12] Ruibo Lu, Qi Hong, Shin-Tson Wu, Kuo-Hsuan Peng, and Hung-Sheng Hsieh. Quantitative comparison of color performances between ips and mva lcds. *IEEE Journal of Display Technology*, 2(4):319–326, 2006.

[13] Xiangyi Nie, Ruibo Lu, Haiqing Xianyu, Thomas X. Wu, and Shin-Tson Wu. Anchoring energy and cell gap effects on liquid crystal response time. *Journal of Applied Physics*, 101:103110, 2007.

[14] Ji Woong Park, Young Joo Ahn, Jun Ho Jung, Seung Hee Lee, Ruibo Lu, Hyang Yul Kim, and Shin-Tson Wu. Liquid crystal display using combined fringe and in-plane electric fields. *Applied Physics Letters*, 93:081103, 2008.

[15] Zhibing Ge, Xinyu Zhu, Thomas X. Wu, and Shin-Tson Wu. High transmittance in-plane switching liquid crystal displays. *IEEE Journal of Display Technology*, 2(2):114–120, 2006.

[16] Daming Xu, Haiwei Chen, Shin-Tson Wu, Ming-Chun Li, Seok-Lyul Lee, and Wen-Ching Tsai. A fringe field switching liquid crystal display with fast grayscale response time. *IEEE Journal of Display Technology*, 11(4), 2015.

[17] A. Lien, C. Cai, R.A John, E. Galligan, and J. Wilson. 16.3q̈sxga high resolution wide viewing angle tft-lcds based on ridge and fringe-field structures. *Displays*, 22(1):9–14, 2001.

[18] Navid Khaledi, Azim Arbabi, and Moloud Dabaghi. X-ray dose estimation from cathode ray tube monitors by monte-carlo calculation. *Health Physics*, 108(4):401–406, 2015.

[19] Marie-Thérése Lecler, François Zimmermann, Eric Silvente, Frédéric Clerc, Alain Chollot, and Jérôme Grosjean. Exposure to hazardous substances in cathode ray tube (crt) recycling sites in france. *Waste Management*, 2015.

[20] H. Kawamoto. The history of liquid crystal displays. *Proceedings of the IEEE*, 90(4):460–500, 2002.

[21] V. Reshetnyak and 0. Shevchuk. Electro-optical characteristics in the in-plane switching of nematic liquid crystals. *Proceedings of SPIE*, 4463, 2001.

[22] Donald Craig. Extensible hierarchical object-oriented logic simulation with an adaptable graphical user interface. Master's thesis, Memorial University of Newfoundland, 1996.

[23] Peter J. Collings and Michael Hird. *Introduction to Liquid Crystals: Chemistry and Physics*. CRC Press, 1997.

[24] M. Schadt and W. Helfrich. Voltage dependent optical activity of liquid crystal. *Applied Physics Letters*, 18:127, 1971.

[25] Eun Jeong, Mi Hyung Chin, Young Jin Lim, Anoop Kumar Srivastava, Seung Hee Lee, Kyung Ho Park, and Hyun Chul Choi. Switching of off-axis viewing quality in twisted nematic liquid crystal display by controlling phase retardation of additional liquid crystal layers. *Journal of Applied Physics*, 104:033108, 2008.

[26] Masahito Oh-e and Katsumi Kondo. Electrooptical characteristics and switching behavior of the in plane switching mode. *Applied Physics Letters*, 67:3895, 1995.

[27] Pochi Yeh and Claire Gu. *Optics of Liquid Crystal Displays*. Wiley Interscience, 1999.

[28] S. H. Lee, S. L. Lee, and H. Y. Kim. Electro-optic characteristics and switching principle of a nematic liquid crystal cell controlled by fringe-field switching. *Applied Physics Letters*, 73:2881, 1998.

[29] André M. Sonnet and Epifanio G. Virga. *Dissipative Ordered Fluids: Theories for Liquid Crystals*. Springer, 2010.

[30] F.C . Frank. On the theory of liquid crystals. *Discussions of the Faraday Society*, 25:19–28, 1958.

[31] R.C. Jones. A new calculus for the treatment of optical systems, i. description and discussion of the calculus. *Journal of the Optical Society of America*, 31(7):488–493, 1941.

[32] A. Lien. Extended jones matrix representation for the twisted nematic liquid crystal display at oblique incidence. *Applied Physics Letters*, 57:2767, 1990.

[33] S. Stallinga. Berreman 4x4 matrix method for reflective liquid crystal displays. *Journal of Applied Physics*, 85:3023, 1999.

[34] Stephen D. Gedney. *Introduction to the Finite-Difference Time-Domain (FDTD) Method for Electromagnetics*. Morgan Claypool, 2011.

[35] J. Van Roey, J. van der Donk, and P. E. Lagass. Beam-propagation method: analysis and assessment. *Journal of the Optical Society of America*, 71(7):803–810, 1981.

[36] M. Becker. Dimos-a software tool for optimizing display systems with lcds. *Displays*, 10(4):215–228, October 1989.

[37] *TechWiz LCD 3D: Multidimensional simulation software for TFT LCD.*

[38] J. Chen, P. J. Bos, D. L. Johnson, D. R. Bryant, J. Li, S.H. Jamal, and J. R. Kelly. Four-domain twisted nematic liquid crystal display fabricated by reverse rubbed polyimide process. *Journal of Applied Physics*, 80:1985–1990, 1996.

[39] Hitoshi Hatoh, Masahito Ishikawa, Junko Hirata, Yuzo Hisatake, and Tomiaki Yamamoto. Improvement of viewing angle characteristics in a twisted-nematic liquid-crystal display by using a cholesteric liquid-crystal compensation layer. *Applied Physica Letters*, 60:1806–1808, 1992.

[40] Kyeong-Hyeon Kim and Jang-Kun Song. Technical evolution of liquid crystal displays. *NPG Asia Materials*, 1:29–36, 2009.

[41] Fabrizio Di Pasquale, F. Anibal Fernandez, Sally E. Day, and J. Brian Davies. Two dimensional finite-element modeling of nematic liquid crystal devices for optical communications and displays. *IEEE Journal Of Selected Topics In Quantum Electronics*, 2(1):128–134, April 1996.

[42] Masahito Oh-e and Katsumi Kondo. Response mechanism of nematic liquid crystals using the in-plane switching mode. *Applied Physics Letters*, 69:623, 1996.

[43] Hiroyuki Mori, Eugene C. Gartland Jr., Jack R. Kelly, and Philip J. Bos. Multidimensional director modeling using the q tensor representation in a liquid crystal cell and its application to the pi cell with patterned electrodes. *Japanese Journal of Applied Physics*, 38(1A):135–146, 1999.

[44] Hyung Jun Yoon, Jun Hee Lee, Min Wan Choi, Jin Woo Kim, Ohseob Kwon, and Taeyoung Won. Comparison of numerical method for analysis of liquid crystal cell: In plane switching. *SID Symposium Digest of Technical Papers*, 34(1):1378–1381, 2003.

[45] Sang Ho Yoon Cheol Soo Lee Suk In Yoon Jun Hee Lee Hyung Jin Yoon Min Wan Choi Jin Woo Kim and Taeyoung Won. Three dimensional numerical simulaton for understanding the fringe field effect on the dynamic behavior of liquid crystal. *Molecular Crystals and Liquid Crystals*, 413(1), 2004.

[46] V. Reshetnyak and 0. Shevchuk. Electro-optical characteristics in the in-plane switching of nematic liquid crystals. *Proceedings of SPIE*, 4463, 2001.

[47] F. A. Fernandez, S. E. Day, P. Trwoga, H.F Deng, and R. James. Three-dimensional modelling of liquid crystal display cells using finite elements. *Molecular Crystals and Liquid Crystals*, 375(1):291–299, 2010.

[48] Haiying Wang, Thomas X. Wu, Xinyu Zhu, and Shin-Tson Wu. Correlations between liquid crystal director reorientation and optical response time of a homeotropic cell. *Journal of Applied Physics*, 95:5502, 2004.

[49] G. Barbero and L.R. Evangelista. *An elementary course on the continuum theory for nematic liquid crystals*. World Scientific, 2001.

[50] B. Wincure and A.D. Rey. Interfacial nematodynamics of heterogeneous curved isotropic-nematic moving fronts. *The Journal of Chemical Physics*, 124:244902, 2006.

[51] Pouya Khayyatzadeh. Geometry and anchoring effects on elliptic cylinder domains of nematic phases. Master's thesis, University of Waterloo, 2014.

[52] Janglin Chen, Wayne Cranton, and Mark Fihn. *Handbook of Visual Display Technology*. Springer, 2012.

[53] Giovanni Barbero and L.R. Evangelista. *Adsorption phenomena and anchoring energy in nematic liquid crystals*. CRC Press, 2005.

[54] Matthijs W. den Otter. Approximate expressions for the capacitance and electrostatic potential of interdigitated electrodes. *Sensors and Actuators A: Physical*, 96(2–3):140 – 144, 2002.

[55] https://launchpad.net/gsml.

[56] I. Nys, J. Beeckman, and K. Neyts. Switchable 3d liquid crystal grating generated by periodic photo-alignment on both substrates. *Soft Matter*, 11:7802, 2015.

[57] http://www.paraview.org/.